Cell Reports

Article

Selective autophagy controls innate immune response through a TAK1/TAB2/SH3PX1 axis

Graphical abstract

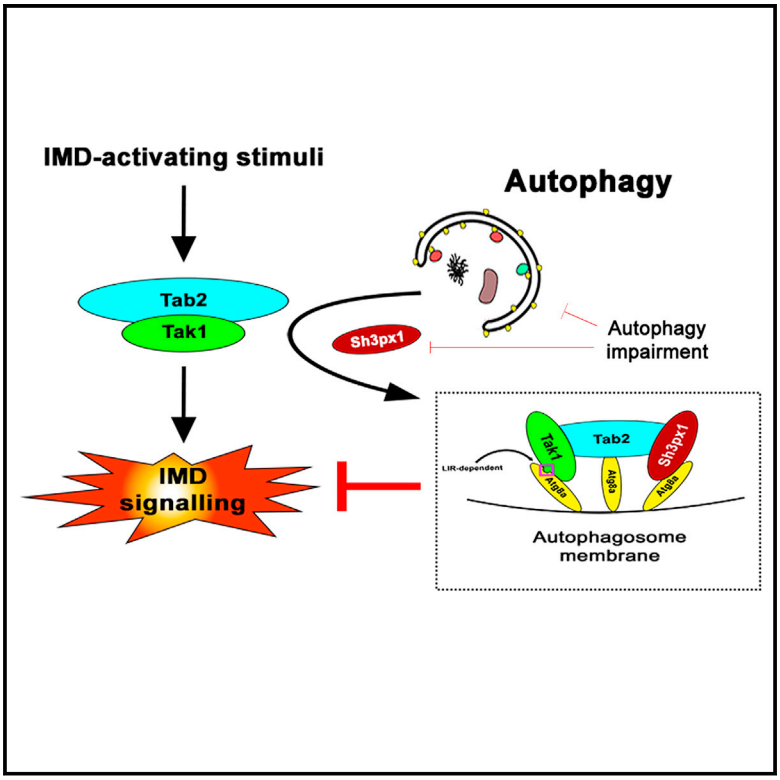

Authors

Panagiotis Tsapras, Stavroula Petridi, Selina Chan, ..., Antonia P. Sagona, Pascal Meier, Ioannis P. Nezis

Correspondence

i.nezis@warwick.ac.uk

In brief

Tsapras et al. perform a yeast-two-hybrid screen to identify Atg8a-interacting proteins in *Drosophila*. They show that Atg8a interacts with TAK1 via an LIR motif. Atg8a also interacts with TAB2. TAB2 interacts with SH3PX1. Selective autophagic degradation of TAK1/TAB2 complex is fine-tuned by SH3PX1 to control innate immune responses.

Highlights

- Yeast-two-hybrid screening identifies Atg8a-interacting proteins
- TAK1 interacts with Atg8a via an LIR motif
- TAB2 interacts with Atg8a and SH3PX1
- Selective autophagic degradation of TAK1/TAB2 complex is fine-tuned by SH3PX1

Tsapras et al., 2022, Cell Reports *38*, 110286
January 25, 2022
https://doi.org/10.1016/j.celrep.2021.110286

CellPress

Cell Reports

CellPress
OPEN ACCESS

Article

Selective autophagy controls innate immune response through a TAK1/TAB2/SH3PX1 axis

Panagiotis Tsapras,[1] Stavroula Petridi,[1,3] Selina Chan,[1,5] Marta Geborys,[1,5] Anne-Claire Jacomin,[1,4] Antonia P. Sagona,[1] Pascal Meier,[2] and Ioannis P. Nezis[1,6,*]

[1]School of Life Sciences, University of Warwick, CV4 7AL Coventry, UK
[2]The Breast Cancer Now Toby Robins Research Centre, Institute of Cancer Research, Fulham Road, London SW3 6JB, UK
[3]Present address: MRC Mitochondrial Biology Unit, The Keith Peters Building, Cambridge Biomedical Campus, Hills Road Cambridge CB2 0XY, UK
[4]Present address: Institute of Biochemistry II, Faculty of Medicine, Goethe University, Frankfurt, Germany
[5]These authors contributed equally
[6]Lead contact
*Correspondence: i.nezis@warwick.ac.uk
https://doi.org/10.1016/j.celrep.2021.110286

SUMMARY

Selective autophagy is a catabolic route that turns over specific cellular material for degradation by lysosomes, and whose role in the regulation of innate immunity is largely unexplored. Here, we show that the apical kinase of the *Drosophila* immune deficiency (IMD) pathway Tak1, as well as its co-activator Tab2, are both selective autophagy substrates that interact with the autophagy protein Atg8a. We also present a role for the Atg8a-interacting protein Sh3px1 in the downregulation of the IMD pathway, by facilitating targeting of the Tak1/Tab2 complex to the autophagy platform through its interaction with Tab2. Our findings show the Tak1/Tab2/Sh3px1 interactions with Atg8a mediate the removal of the Tak1/Tab2 signaling complex by selective autophagy. This in turn prevents constitutive activation of the IMD pathway in *Drosophila*. This study provides mechanistic insight on the regulation of innate immune responses by selective autophagy.

INTRODUCTION

The anti-inflammatory pathways of the host innate immune response comprise the most ancient system of a frontline multi-layered defense against invading pathogens. Signaling and mediation of the desired effects for most of these pathways is carried out by members of the nuclear factor-kappa B (NF-kB) superfamily of transcription factors (Buchon et al., 2014). These NF-kB-associated cascades culminate in the transient and acute expression of immune- and stress-response genes, whose products are aimed toward neutralizing the foreign threat but can also have cytotoxic effects for cells if not properly turned over (Buchon et al., 2014). The aberrant and unwarranted activation of NF-kB-mediated immune cascades, in particular, is largely responsible for the chronic low-grade inflammatory signaling that underlies aging in many species, including humans, and is linked to its most detrimental side effects (Franceschi et al., 2006; Salminen et al., 2008). As such, there is an elaborate network of crosstalking components and pathways that oversee the strict spatiotemporal regulation of NF-kB immune pathways, to maintain a homeostatic intracellular environment. One part of this regulatory network is autophagy; a housekeeping process that aids in the fine-tuning of innate immune signaling cascades (Deretic, 2021). Among its other functions, autophagy has been shown to have a role in dampening the NF-kB signal of innate immune responses against invading pathogens, or cytosol-detected DNA of mitochondrial or viral origin (Nakahira et al., 2011; Prabakaran et al., 2018; Tusco et al., 2017). This is achieved by removing key signal transduction components from these cascades (Nakahira et al., 2011; Prabakaran et al., 2018; Tusco et al., 2017).

Autophagy is an evolutionary conserved process by which cells degrade parts of themselves via the lysosome, and, together with its sister pathway, endocytosis, they constitute the two major routes of intracellular vesicle trafficking (Tooze et al., 2014). Macro-autophagy, in particular (hereafter referred to as autophagy), sequesters cellular material into signature double-membrane vesicles called autophagosomes. The cargo-loaded autophagosomes then fuse with lysosomes, whereupon they, along with their contents, are degraded by the resident hydrolases and any essential building blocks are subsequently recycled back to the cytosol to fuel other metabolic pathways (Parzych and Klionsky, 2014). Autophagy's most recognizable physiological role is as a survival response against environmental nutrient scarcity that counterbalances the depletion of intracellular energy stores through the bulk degradation of non-vital intracellular constituents. Under basal conditions, autophagy participates in cellular upkeep by selectively removing target substrates such as misfolded proteins and protein aggregates, as well as damaged or long-lived organelles (Mizushima, 2007). Intracellular constituents that signal for their selective pick-up by the autophagic machinery

in turn are known as selective autophagy receptors (SARs) (Johansen and Lamark, 2020). They interact with members of the autophagy-related (Atg)-8 family of proteins (Atg8/light chain 3 [LC3]). For this purpose, most SARs contain one or more short peptide sequences called LC3-interacting regions (LIRs; for mammals and other higher eukaryotes), or Atg8-interacting motifs (AIMs; terminology mostly used in yeast) (Birgisdottir et al., 2013; Johansen and Lamark, 2011). Of the multiple LIR sequences on typical SARs, often one is the dominant motif, which mediates docking to its cognate LIR docking site (LDS) on Atg8/LC3 at the autophagosome membrane (Birgisdottir et al., 2013; Johansen and Lamark, 2011).

The molecular determinants that link selective autophagy of cellular self-components with innate immunity remain largely unexplored. Toward this goal, we focus our investigations in the *Drosophila* immune deficiency (IMD) innate immune response, which shares many similarities with TNFR signaling in mammals (Buchon et al., 2014). The IMD pathway regulates expression of most antimicrobial peptides (AMPs) in the fruit fly and is predominantly induced by gram-negative (gram^{-ve}) bacteria (Myllymaki et al., 2014). Very briefly, activation of the surface receptor leads to the intracellular recruitment of receptor-proximal adaptor protein such as the namesake Imd, and transforming growth factor (TGF) beta-activated kinase 1 (Tak1)-binding protein 2 (Tab2) (Kleino et al., 2005). Tab2 binds to and co-activates the apical IMD-signaling kinase, Tak1 (Silverman et al., 2003; Zhuang et al., 2006), which in turn phosphorylates the IKK regulatory subunit Kenny (IKKγ in mammals) and promotes activation of the IKK complex (Rutschmann et al., 2000; Stöven et al., 2003). The inflammatory signal propagates downstream to the cytosol-localized transcription factor Relish (*Drosophila* homolog of mammalian NF-kB) and culminates with the translocation of activated Relish to the nucleus, where it drives expression of IMD-regulated AMP genes, most notably members of the *Attacin* (*Att*), *Diptericin* (*Dpt*) and *Drosocin* (*Dro*) families (Imler and Bulet, 2005). Expression of *DptB*, in particular, is under the control of IMD and as such is often used as a readout of the pathway's activation (Imler and Bulet, 2005; Tanji et al., 2007).

We have screened the *Drosophila* proteome to identify proteins that interact with Atg8a via the use of a high-throughput yeast-two-hybrid (Y2H) screening. The results of this large-scale analysis included targets that have been already experimentally verified to bind Atg8a/LC3, as well as undescribed Atg8a-interacting proteins, such as tricornered/serine/threonine-protein kinase 38 (Trc/STK38) and Tak1. In this work we aimed to further delineate the molecular interactions between selective autophagy and the IMD pathway at the level of Tak1. Based on our observations, we report that Tak1 and its co-activator, Tab2, both interact with Atg8a. Our results show that Tak1 is selectively targeted for elimination by autophagy. In addition, we identified that *Drosophila* sorting nexin Src-homology 3 and Phox -homology domain-containing protein 1 (Sh3px1) is a binding partner of Tab2 and required for the effective regulation of the IMD pathway at the level of Tak1/Tab2. Overall, the results of this work provide further insight into the underlying network of regulatory interactions that contribute to the fine-tuning of the IMD pathway by selective autophagy.

RESULTS

Identification of Atg8a-interacting proteins by Y2H screening

In order to identify Atg8a-interacting proteins in *Drosophila*, we performed a Y2H screening using *Drosophila* Atg8a (1–121), as a LexA-bait (pB27) and an inducible LexA-bait fusion (pB31), performed on a *Drosophila* third instar larvae library. The analysis yielded several Atg8a-interacting proteins (Table S1) in over 103 million interactions tested. In addition, for each of those positive hits, the screen mapped a region termed selected interaction domain (SID), which corresponded to where the Atg8a binding was detected (Figures S1 and S2). We classified these interactions into three groups: (1) proteins that had already been experimentally verified to bind Atg8a, such as Atg1 (Alemu et al., 2012), diabetes and obesity regulated (Dor) (Francis et al., 2010; Nowak et al., 2009), refractory to Sigma P (Ref(2)P) (Jain et al., 2015), and Kenny (Tusco et al., 2017); (2) *Drosophila* proteins for which their mammalian homologs are known to associate with ATG8-family members, such as Ankyrin 2 (Ank2) (Li et al., 2018), Atg4a (Kirisako et al., 2000), and neural precursor cell-expressed developmentally down-regulated protein 4 (Nedd4) (Sun et al., 2017); and (3) undescribed Atg8a-interacting proteins (Figures S1 and S2; Table S1), such as Trc and Tak1. In order to corroborate the initial Y2H results for group III at this early stage, we conducted follow-up glutathione S transferase (GST)-pulldown experiments for Trc as means of proof. We observed that the 6xHis (His)-tagged Trc prey co-precipitated with the wild-type (WT) recombinant GST:Atg8a bait, indicating a direct protein-protein interaction (Figure S3A). This interaction was maintained even after substituting GST:Atg8a^{WT} for a K48A/Y49A LDS inactive mutant form (Atg8a^{LDS}), which is unable to recognize and bind LIR motifs. This suggests that Trc interacts with Atg8a without the need of an LIR motif. Complementing these *in vitro* observations, confocal imaging of fat body tissue (fly organ equivalent to mammalian liver) from *Drosophila* larvae co-expressing upstream-activating sequence (UAS)-Trc:GFP and the autophagic marker mCherry:Atg8a, provided evidence for Trc colocalizing with Atg8a following induction of autophagy (Figure S3B).

Taken together, the above experimental observations provide a level of confidence for the validity of the Y2H-identified Atg8a-interacting proteins of group III by indicating that Trc interacts with Atg8a both *in vitro* and *in vivo*. In addition, our findings suggest that Trc and Atg8a interact via non-LDS/LIR-mediated means.

Tak1 is an Atg8a-interacting protein

In our ongoing effort to delineate the regulatory interactions between components of the IMD immune response and autophagy, we have previously demonstrated that the regulatory subunit of the *Drosophila* IKK complex, Kenny, binds Atg8a in an LIR-dependent manner (Tusco et al., 2017). Prompted by the identification of Tak1 as a candidate Atg8a-interacting protein in the Y2H screen (Figure S1; Table S1), here we tested the ability of Tak1 to interact with Atg8a. The Y2H-mapped SID region that mediates the proposed interaction of the kinase with Atg8a spans the last 116 amino acids of the Tak1 C terminus (Figure 1A). We employed a computational approach to identify

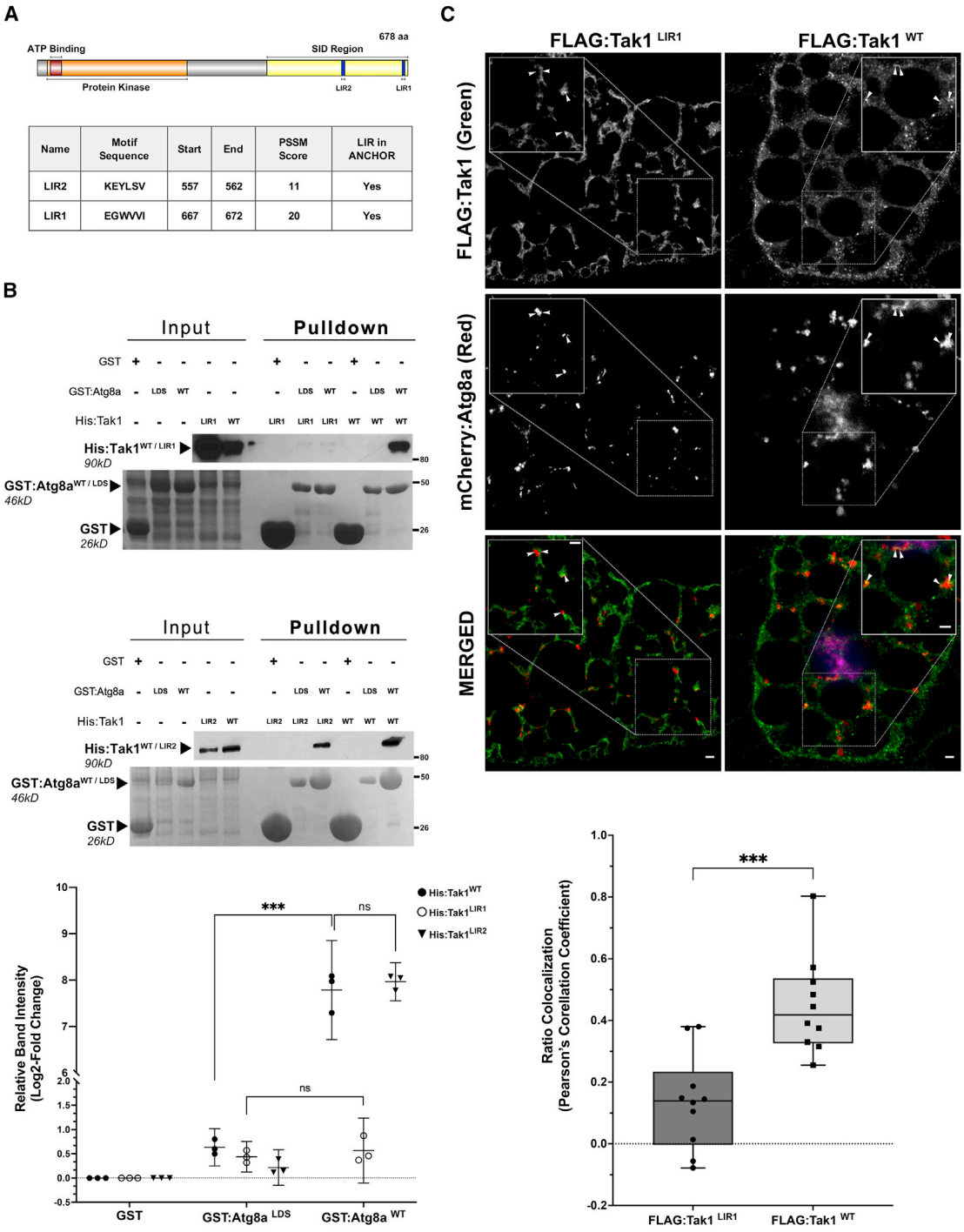

Name	Motif Sequence	Start	End	PSSM Score	LIR in ANCHOR
LIR2	KEYLSV	557	562	11	Yes
LIR1	EGWVVI	667	672	20	Yes

Figure 1. *Drosophila* Tak1 interacts with Atg8a via a functional LIR motif

(A) 2D domain organization of *Drosophila* Tak1. SID refers to the region where binding of Atg8a was mapped, according to Y2H screen. Candidate LIR motifs nested within the SID region are also shown with their details depicted in the table below.

(B) Affinity of Tak1 LIR1 and LIR2 motifs for Atg8a assessed by GST pulldown. GST:bait and His:prey samples were co-incubated in the combinations shown above each gel image. Further presence or absence of proteins is indicated by (+) or (−) respectively. LIR1, LIR2, and LDS refer to the inactive mutant isoform for each protein, while WT indicates the normal protein. Quantification of binding affinity shown below image. Data shown as individual Log2 values with mean ± 95% confidence interval (CI; n = 3 independent biological repeats; statistical analysis by unequal variance one-way ANOVA with Dunnett correction for multiple comparisons; ***$p < 0.001$; ns, not significant, $p > 0.05$).

(legend continued on next page)

candidate LIR motifs on the Tak1 protein sequence using the previously developed iLIR software (Kalvari et al., 2014). This LIR pattern prediction tool identified two candidate motifs whose positions were entirely nested within the Tak1 SID region returned by Y2H (Figures 1A and S2; Table S1). The high position specific scoring matrix (PSSM) value (Figure 1A; Table S1) for each of the two LIR peptides indicates that their amino acid sequences are considered as conserved among LIR motifs (Birgisdottir et al., 2013). Numbered from highest to lowest PSSM score, these LIR motifs are at positions 667–672 (EGWVVI; LIR1), and 557–562 (KEYLSV; LIR2). In order to assess their functionality, we created inactive LIR mutants by substituting the aromatic and hydrophobic residues at positions 3 and 6 respectively with alanine (W669A/I672A for LIR1; Y559A/V567A for LIR2). These positions are largely stringent across canonical LIR motifs in terms of the amino acids they can accommodate, as they are key in controlling the affinity of LIRs for the LDS pocket of Atg8a/LC3 (Birgisdottir et al., 2013). Substitution by amino acids of different properties, such as the neutral A, results in marked reduction to abolishment of the ability for an LIR peptide to dock to LDS, rendering the LIR motif non-functional (Birgisdottir et al., 2013). We introduced each inactive LIR mutant (hereafter Tak1^{LIR1} and Tak1^{LIR2} in figures and text and referring to the Tak1$^{W669A/I672A}$ and Tak1$^{Y559A/V562A}$ mutant LIR isoforms respectively) into GST-pulldown assays with Atg8a, alongside normal Tak1 and the inactive LDS form of Atg8a (Figure 1B). We observed that His:Tak1^{WT} directly binds to GST:Atg8a^{WT} and this interaction is abolished in the presence of the mutant GST:Atg8a^{LDS} isoform (Figure 1B). Similarly, neither His:Tak1 LIR mutant prey was able to co-precipitate with GST:Atg8a^{LDS}, and we also did not detect any association for either His:Tak1 prey with the unconjugated GST tag alone (Figure 1B). Taken together, this indicates that binding between Tak1 and Atg8a is specific, as the GST tag does not influence their co-association, and it represents an LDS/LIR-dependent mode of interaction. Furthermore, we observed that inactivation of the Tak1 LIR1 motif resulted in near-total loss of the interaction between the kinase and GST:Atg8a^{WT}, while, in contrast, no similar reduction in signal strength was observed for the His:Tak1^{LIR2} mutant isoform (Figure 1B). These results, show that the LIR1 motif mediates the interaction between Tak1 and Atg8a.

In order to investigate the functional relevance of the Tak1 LIR1 motif, we created transgenic flies that ectopically express either a 3xFLAG (FLAG):Tak1^{WT} or FLAG:Tak1^{LIR1} construct. Both constructs are under the control of an inducible UAS promoter. We co-expressed each transgene in the larval fat body together with mCherry:Atg8a and induced autophagy by nutrient deprivation (Figure 1C). After immunofluorescence imaging and follow-up quantitative analysis, we observed that FLAG:Tak1^{WT} frequently formed small cluster regions and often colocalized with mCherry:Atg8a on punctate formations resembling autophagosomes, while its LIR1 mutant counterpart did so to a considerably lesser extent (Figure 1C). That difference was maintained under the same autophagy-inducing conditions when using cathepsin-L as a marker for lysosomes (Figure S4). We found both FLAG:Tak1^{WT} and FLAG:Tak1^{LIR1} were encountered near the vicinity of lysosome-rich regions; however, FLAG:Tak1^{WT} seemingly displayed increased affinity for lysosomes compared with FLAG:Tak1^{LIR1} (Figure S4). This suggests that the LIR1 motif of Tak1 favors the association of the TAK1 with autophagosomes and lysosomes.

In summary, here we corroborated the Y2H screen result of Tak1 interacting with Atg8a and further proceeded to characterize that this is an LIR/LDS-dependent interaction, facilitated by the 667-EGWVVI-672 LIR1 motif of Tak1.

Tak1 is degraded by autophagy and this is required for downregulation of the IMD pathway

The observed LIR/LDS-dependent interaction between Tak1 and Atg8a prompted us to examine whether basal autophagy has a role in degrading Tak1, and how that may translate to the IMD pathway signaling in cases where autophagy is inhibited or perturbed. For this purpose, we first investigated if the Tak1 protein amount varies between normally fed, young (1 week), and old (3 week) adult WT and autophagy-deficient (*Atg8a*^{KG07569}; hereafter Atg8a) flies. We used the accumulation of the SAR Ref(2)P (fly homolog of mammalian SQSTM1/p62 adaptor) as a routinely employed positive marker to indicate autophagy dysfunction as shown before (Mauvezin et al., 2014; Nezis et al., 2008). We ran samples on SDS-PAGE, followed by western blot and staining with an anti-Tak1 antibody. Subsequent densitometric and statistical analysis of the normalized data revealed that the Tak1 protein is more abundant in *Atg8a*-mutant flies compared with WT controls (Figures 2A and 2B). In immunofluorescence imaging of larval fat bodies from normally fed WT and Atg8a flies that were co-stained for Ub and endogenous Tak1, we observed a similar phenotype of protein aggregation in the Atg8a samples (Figures 2C and 2D). More specifically, under normal feeding conditions, Atg8a flies formed distinct Ub aggregates (Figure 2C), which is characteristic of impaired autophagic turnover in these flies, as shown before (Bjørkøy et al., 2005; Kirkin et al., 2009; Komatsu et al., 2006; Nezis et al., 2008; Pankiv et al., 2007). Furthermore, Tak1 seemed to form similar protein aggregates to Ub in these *Atg8a*-mutants, which were spread throughout the fat body tissue and occasionally colocalized with Ub in the same protein inclusions (Figure 2C). The WT larvae by comparison displayed a more diffuse staining for both Ub and Tak1 (Figure 2C). We used a semi-automated method to quantify the Tak1 puncta

(C) Confocal imaging of fat body cells from *Drosophila* third instar larvae co-expressing mcherry:Atg8a and either FLAG:Tak1^{LIR1} or FLAG:Tak1^{WT}. Focus areas in each image depict a representative region of the sample where the Atg8a and Tak1 signals overlap. For the Tak1^{LIR1} sample, the two top-most arrowheads show a region of colocalization (right arrow) as well as a region of mutual exclusion (left arrow) for the Atg8a and Tak1 signals. Scale bar: 2 μm. Degree of colocalization (Pearson's R) between mcherry:Atg8a and FLAG:Tak1$^{LIR1/WT}$ shown below image. Data shown as mean ± 95% CI in distribution boxplot with individual R values (n = 10; where n is the number of confocal images analyzed from independent samples for each condition; statistical analysis by equal variance unpaired t test; ***$p < 0.001$).

Genotypes for (C): *yw hs-Flp;Ac > CD2 > GAL4/+;UAS-mCherry-Atg8a/UAS-3xFLAG:Tak1^{WT}* and *yw hs-Flp;Ac > CD2 > GAL4/+;UAS-mCherry-Atg8a/UAS-3xFLAG:Tak1^{LIR1}*

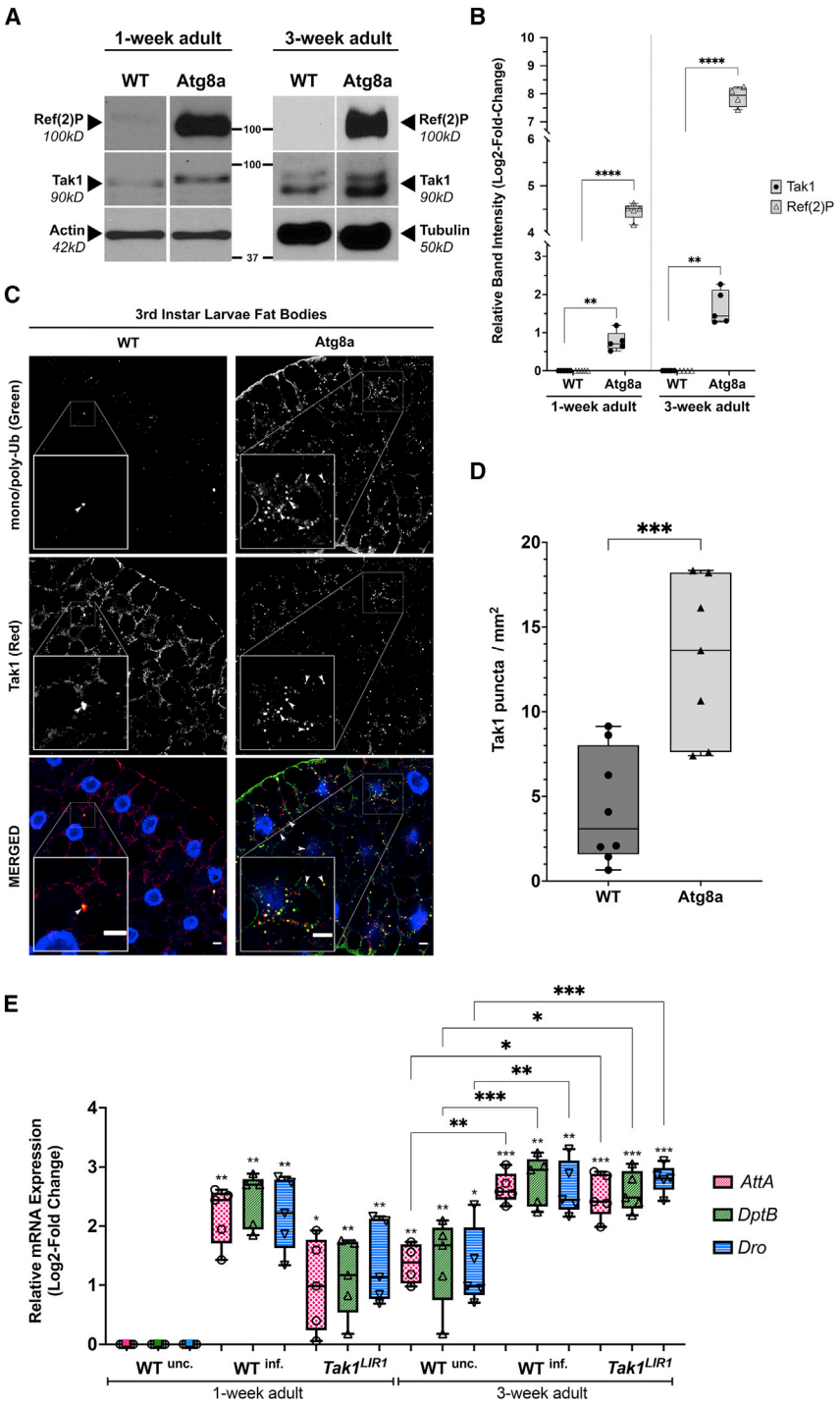

Figure 2. Tak1 is degraded by autophagy and controls IMD downregulation

(A) Western blot of whole-fly protein extracts for detecting endogenous Ref(2)P and Tak1 in young and old WT and Atg8a flies.

(B) Quantification of Tak1 and Re(2)P band intensity in young and old WT and Atg8a flies. Data shown as median ± 95% CI in distribution boxplot with individual Log2 values (n = 4–5 independent biological repeats; statistical analysis by one-sample t test; **p < 0.01; ****p < 0.0001).

(C) Confocal imaging of *Drosophila* fat body cells from third instar WT and Atg8a larvae, co-stained for Tak1 (red) and Ub (green) following autophagy upregulation. Arrowheads within focus areas from widefield regions point toward aggregates positive for Ub and Tak1. Scale bar: 5 μm.

(D) Quantification of Tak1 puncta per mm^2 of fat body tissue. Data shown as median ± 95% CI in distribution boxplot with individual values (n = 7–8 representative confocal images analyzed from independent samples for each condition; statistical analysis by equal variance unpaired t test; ***p < 0.001).

(E) RT-qPCR for mRNA levels of selected AMP genes in young and old $Tak1^{LIR1}$ flies. $WT^{unc.}$ used as reference groups and $WT^{inf.}$ as positive controls for activation of IMD after microbial infection. Data shown as median ± 95% CI in distribution boxplot with individual Log2 values (n = 5 independent biological repeats; statistical analysis by one-sample t test for comparisons with the 1-week $WT^{unc.}$ group and by equal variances one-way ANOVA with Bonferroni correction test for comparisons within the 3-week adult group; *p < 0.05; **p < 0.01; ***p < 0.001).

Genotypes for (A)–(D): w^{1118} (WT), $Atg8a^{KG07569}$ (Atg8a).

Genotype for (E): *Tak1* $LIR^{W669A/I672A}$ ($Tak1^{LIR1}$).

in each image and found that these were significantly enriched per square millimeter in fat body cell images of Atg8a flies compared with WT (Figure 2D). To corroborate our findings that Tak1 forms numerous and distinct protein inclusions under instances of impaired autophagic clearance in general and not specifically by genetic inhibition of the process, we induced chemical inhibition of autophagy by raising WT larvae in fly food containing 10 mg/mL (w/v) chloroquine (CQ). WT controls were raised in normal fly food. The Ub and Tak1 aggregation phenotype observed in the fat bodies of Atg8a flies was also extensively mimicked by the CQ-treated WT flies in contrast to controls (Figure S5).

Altogether, the results from these combinatory biochemical and immunofluorescent approaches show that Tak1 constitutes a substrate for degradation by autophagy.

We have previously shown that autophagy attenuates the IMD response by selectively degrading the IKK complex via the interaction of its regulatory subunit Kenny with Atg8a (Tusco et al., 2017). Our findings so far in this work suggest that autophagy may have an even more extensive role in the downregulation of IMD than previously thought, by acting at the upper tier of the signaling cascade to remove the apical kinase, Tak1, through an association that is at least in part facilitated by the LIR1 motif

on the kinase. As such, we investigated whether impairing autophagy's recruitment through the Tak1 LIR1 motif by inactivating it may subsequently have any measurable effect on the chronic regulation of the IMD immune pathway across aging flies. We utilized CRISPR-mutant flies in RT-qPCR assays, where the $Tak1^{WT}$ gene has been rendered into the inactive LIR mutant $Tak1^{LIR1}$. We measured the systemic mRNA levels of the *Drosophila* AMP family members *AttA*, *DptB*, and *Dro* in population samples of unchallenged young (1 week) and old (3 week) adult WT ($WT^{unc.}$) and $Tak1^{LIR1}$ flies. These AMP genes are predominantly active against $gram^{-ve}$ bacteria and, as such, their transcription is directly dependent on the IMD pathway's state of activation (Engström, 1999; Hanson et al., 2019; Lemaitre et al., 1997). We employed WT flies transiently infected ($WT^{inf.}$) with the $gram^{-ve}$ mild pathogenic bacteria *Ecc15* (Basset et al., 2000), as positive controls for the induction of IMD, in response to acute microbial challenge.

Following analysis of our qPCR data, we observed that AMP levels for all the genes tested were significantly elevated in both age groups and across conditions, compared with 1-week $WT^{unc.}$ flies (Figure 2E). As expected, $WT^{inf.}$ flies show pronounced upregulation of IMD-controlled AMP genes, indicating the transient hyperactivation of the inflammatory response following microbial infection (Figure 2E). Interestingly, we observed that systemic mRNA levels of each AMP tested were also more abundant in otherwise unchallenged young adult (1 week) $Tak1^{LIR1}$ flies (Figure 2E). The mRNA amount of each AMP gene was found to be two to four times greater relative to their corresponding level in the $WT^{unc.}$ control group of the same age (Figure 2E). We also note that AMP levels of these young adult $Tak1^{LIR1}$ flies are directly comparable with the elevated amounts observed in the older $WT^{unc.}$ flies (Figure 2E), which indicates the chronic low-grade overactivation of the innate immune response during aging in flies and mammals (Franceschi et al., 2017; Zerofsky et al., 2005). This underlying systemic inflammation seems to be even more exacerbated in the unchallenged old $Tak1^{LIR1}$ flies compared with their age-matched $WT^{unc.}$ controls (Figure 2E).

The Toll pathway is the other major branch of the innate immune defense against external microbial pathogens, and is primarily activated by $gram^{+ve}$ bacteria and fungi (Valanne et al., 2011). We examined if Toll also shared IMD's observed reliance on autophagy for the effective downregulation of its signaling and, consequently, if it displayed evidence of hyperactivation upon inhibition of autophagy. To do this, we measured relative protein amounts in western blot between old (3-week-old adult) WT and Atg8a flies for the Toll-specific transcription factor Dorsal and its regulatory IκB partner Cactus (Valanne et al., 2011). We did not observe either Cactus or Dorsal displaying any significant difference in their relative protein amount in Atg8a flies compared with their age-matched WT counterparts (Figure S6A). This indicates that the Toll pathway is arguably less sensitive on autophagy manipulations compared with IMD. It therefore seems that, of the two innate immune pathways, autophagy's regulatory control is targeted more towards IMD than Toll.

Collectively, these observations suggest that, under basal conditions, the Tak1 LIR1 motif has a role in preventing the constitutive overactivation of the IMD response in *Drosophila*, via a mechanism that involves the selective autophagic degradation of Tak1 through the LIR-dependent interaction of Tak1 with Atg8a.

Tab2 interacts with Atg8a and is a substrate for autophagy

To propagate the IMD signal further downstream, activation of TAK1 in flies and mammals requires the association of the kinase in a stable complex with its co-activating adaptor protein TAB2 (Besse et al., 2007; Zhuang et al., 2006).

So far, we have found that Tak1 was identified by the Y2H for Atg8a interactors (Figure S1; Table S1), can associate directly with Atg8a in an LIR/LDS-dependent manner (Figure 1), and is a substrate for autophagic clearance (Figure 2). Although its binding partner Tab2 was not identified in the initial Y2H screen, its strong relationship with Tak1 and the prediction of two conserved LIR motifs in its sequence (Figure 3A) provided reasonable grounds to examine if Tab2 is nevertheless able to crosstalk with components of the autophagic machinery. We noted that Tab2 displays evidence of accumulation in old, autophagy-impaired *Atg8a*-mutant flies, following western blot analysis (Figure 3B). By employing GST-pulldown assays, we observed that *in vitro*-translated $His:Tab2^{WT}$ is capable of binding directly to $GST:Atg8a^{WT}$ (Figure 3C). Neither co-incubation with a $GST:Atg8a^{LDS}$ bait nor inactivation of either of the candidate LIR motifs on Tab2 (F339A/I342A for LIR1, and F372A/L375A for LIR2) resulted in any significant loss in the affinity of Tab2 for Atg8a (Figure 3C). This suggests an LIR motif-independent mode of interaction between the two proteins. We next attempted to identify the domain on Tab2 that mediates interaction with Atg8a. For this purpose, we created two His:Tab2 protein fragments ($His:Tab2^{1–336}$ and $His:Tab2^{376–831}$, hereafter referred to in text and figures as $His:Tab2^{N'}$ and $His:Tab2^{C'}$ respectively, pertaining to the inclusion of the N'-, or C'-terminal domain of the full protein). We ensured that both Tab2 LIR1 (amino acid position 337–342) and LIR2 (amino acid position 370–375) motifs were missing from each construct. Introducing these constructs into GST pulldown, we observed that $His:Tab2^{N'}$, but not $His:Tab2^{C'}$, was able to co-precipitate in the presence of either $GST:Atg8a^{LDS}$ or $GST:Atg8a^{WT}$ in comparable amounts (Figure 3D). This further supports that Tab2 can bind Atg8a without the need for an LIR motif and indicates that the responsible domain for mediating this interaction lies within the 1–336-amino acid region of the Tab2 protein.

Taking all the above into consideration, our findings suggest that Tab2 is a substrate for autophagic clearance. Furthermore, we report that N-terminal 1–336 region of Tab2 interacts directly with Atg8a.

The sorting nexin Sh3px1 binds Tab2 and regulates the IMD pathway across the *Drosophila* lifespan

The *Drosophila* sole representative of the mammalian sorting nexin (SNX)9/18/33-family, Sh3px1, has been known to interact with Atg8a and be a necessary component during autophagosome formation by maintaining membrane curvature of the developing structure (Knævelsrud et al., 2013). Using a proteomic-based approach to identify Tab2-interacting proteins, we observed that Sh3px1 selectively co-purified with Tab2 isolated from *Drosophila*

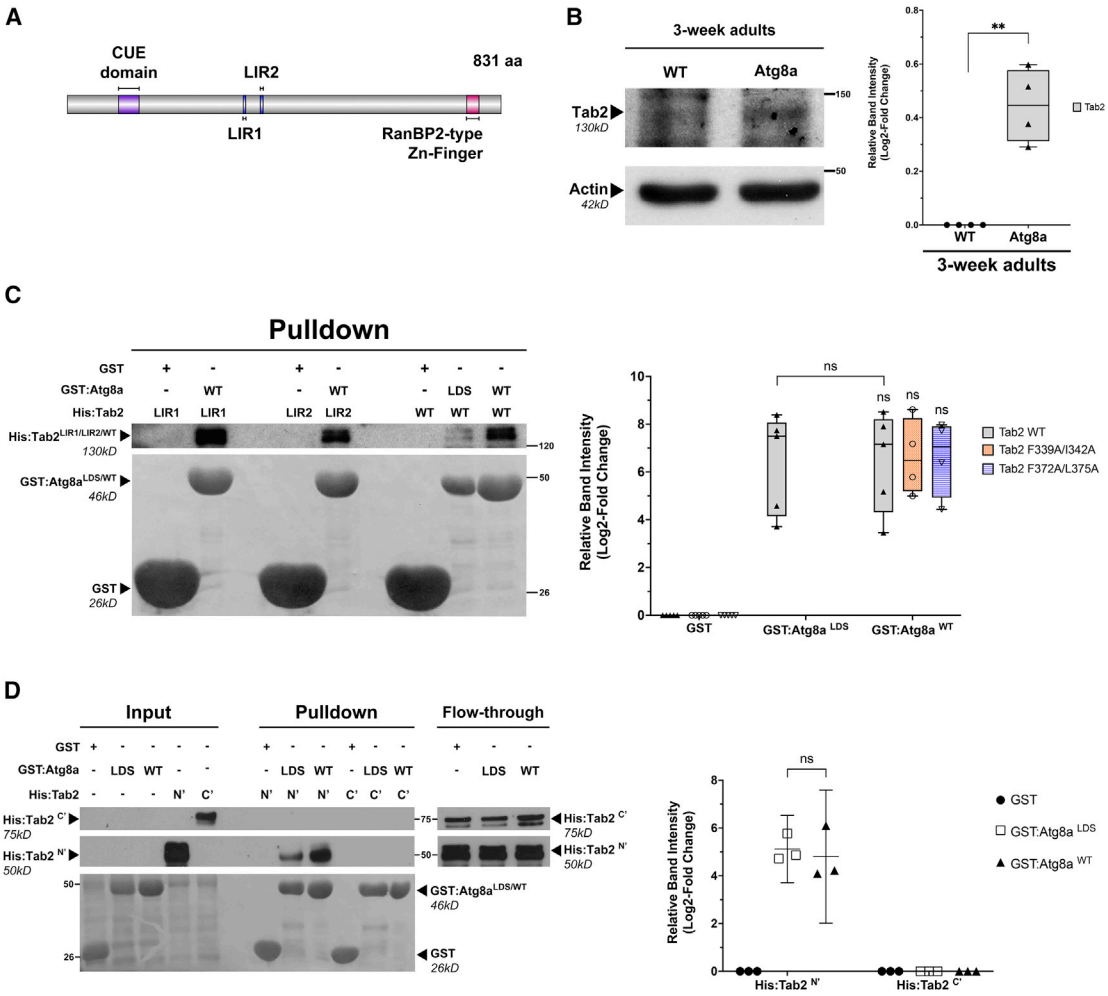

Figure 3. *Drosophila* Tab2 binds Atg8a and is a substrate for autophagic clearance

(A) 2D domain organization of Tab2. Details of the candidate LIR motifs for mediating interaction with Atg8a are shown in the table below.

(B) Western blot of whole-fly protein extracts for detecting endogenous Tab2 in old WT and Atg8a flies. Quantification plot shown on right of image. Data shown as median ± 95% CI in distribution boxplot with individual Log2 values (n = 4 independent biological repeats; statistical analysis by one-sample t test; $^{**}p < 0.01$).

(C) Affinity of Tab2 LIR1 and LIR2 motifs for Atg8a assessed by GST pulldown. GST:bait and His:prey samples were co-incubated in the combinations shown above each gel image. Further presence or absence of proteins is indicated by (+) or (−) respectively. LIR1, LIR2, and LDS refer to the inactive mutant isoform for each protein, while WT indicates the normal protein. Quantification of binding affinity shown on the right of image. Data shown as median ± 95% CI in distribution boxplot with individual Log2 values (n = 4–5 independent biological repeats; statistical analysis by equal variance one-way ANOVA with Bonferroni correction for multiple comparisons; ns, not significant, $p \geq 0.05$).

(D) GST pulldown for recombinant Tab2 fragments His:Tab2$^{N'}$ and His:Tab2$^{C'}$ to determine the Tab2 interaction domain with Atg8a. Quantification of binding affinity for each fragment shown on the right of image. Data shown as individual Log2 values with mean ± 95% CI (n = 3 independent biological repeats; statistical analysis by equal variance unpaired t test; ns, not significant, $p \geq 0.05$).

Genotypes for (B): w^{1118} (WT), $Atg8a^{KG07569}$ (Atg8a).

S2 cells, with a high confidence significance analysis of interactome (SAINT) (Choi et al., 2011) score of 1 (Figure 4A). Under the same conditions, Sh3px1 was not co-purified by either IMD, Fadd, Dredd, Ird5, Kenny, or Relish (SAINT score of 0, data not shown). This was a particularly interesting finding for our study, especially since the sorting nexin has previously been implicated in the regulation of proliferation rate of intestinal stem cells (ISCs) in the fly midgut (Zhang et al., 2019). To contextualize this observation, it is important to note here that the gut epithelia is host to many commensal microbiota populations, as well as a regular target for invading pathogens via food ingestion (Buchon et al., 2009; Ryu et al., 2008). Under normal circumstances, ISCs activate in order to replace epithelial cells that have been damaged during acute inflammatory challenges, and this serves as a marker of an upregulated immune response in the gut (Buchon et al., 2009; Ryu et al., 2008). On the other hand, uncontrolled ISC proliferation contributes to gut dysplasia and is, by extent, a characteristic signature of the deregulated immune signaling, which underlies chronic inflammation in aging flies (Biteau et al., 2010; Buchon et al., 2009; Guo et al., 2014; Ryu et al., 2008). Although Sh3px1 has

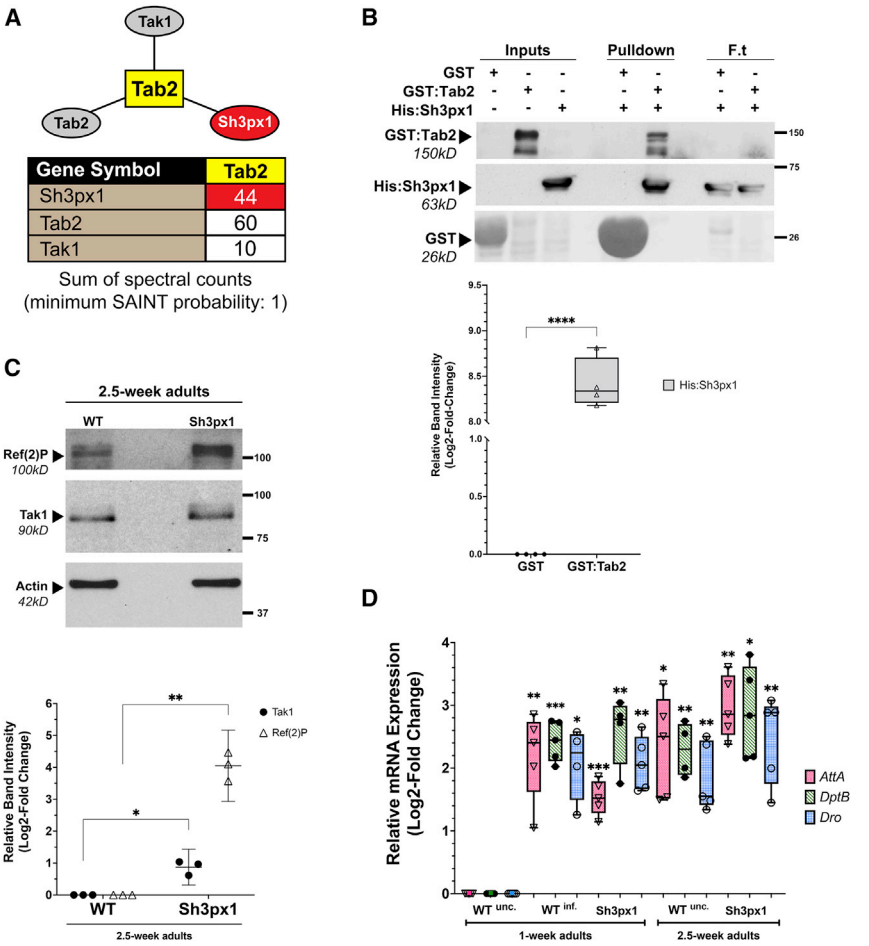

Figure 4. Sh3px1 binds Tab2 and is a regulator of the IMD pathway

(A) Schematic representation of the Tab2-bound target proteins identified by mass spectrometry. Table specifies the sum of spectral counts with a SAINT score probability of 1.

(B) GST-pulldown assay to investigate the interaction between GST:Tab2 and His:Sh3px1. GST:bait and His:prey were co-incubated in the combinations indicated by the table above each gel, with (+) referring to presence and (−) denoting absence of the specific protein from the gel-loading sample. Quantification plot shown below image. Data shown as median ± 95% CI in distribution boxplot with individual Log2 values (n = 4 independent biological repeats; statistical analysis by one-sample t test; ****$p < 0.0001$).

(C) Western blot of whole-fly protein extracts for detecting endogenous Tak1 and Ref(2)P in old WT and Sh3px1 flies. Quantification plot shown below image. Data shown as individual Log2 values with mean ± 95% CI (n = 3 independent biological repeats; statistical analysis by one-sample t test; *$p < 0.05$; **$p < 0.01$).

(D) RT-qPCR for mRNA levels of selected AMP genes in young and old Sh3px1 flies. $WT^{unc.}$ used as reference groups and $WT^{inf.}$ as positive controls for activation of IMD after microbial infection. Data shown as median ± 95% CI in distribution boxplot with individual Log2 values (n = 5 independent biological repeats; statistical analysis by one-sample t test for comparisons with the 1-week $WT^{unc.}$ group; *$p < 0.05$; **$p < 0.01$; ***$p < 0.001$).

Genotypes for (C)–(D): w^{1118} (WT), $Sh3px^{10A/C1\ CRISPR\ E2}$ (Sh3px1).

been associated as such with control of the ISC proliferation, it is still unclear how the sorting nexin specifically exerts its regulatory effects on innate immune response. The apparent existence of a mechanistic link between Sh3px1 and Tab2 provided compelling evidence for a direct role of the sorting nexin in regulating the IMD immune response at the upper tier of the signaling cascade. Combined with its documented function in autophagy, we proceeded to investigate this relationship further and delineate how exactly Sh3px1 might regulate activation of the IMD pathway at the level of the apical Tak1/Tab2 kinase complex.

In addition to mass spectrometry analysis, we also confirmed the Tab2-Sh3px1 interaction via GST-pulldown assays (Figure 4B). Small amounts of recombinant GST:Tab2 were able to strongly precipitate His:Sh3px1, highlighting that the two proteins are able to associate together via a specific and direct interaction (Figure 4B). To study the effect of loss of *Sh3px1* on the functionality of autophagy, we ran samples of old (2.5-week-old adult) WT and *Sh3px1*-null ($Sh3px1^{10A/C1}$; hereafter Sh3px1) flies in western blot and stained for Ref(2)P. We observed that loss of *Sh3px1* did account, to a degree, for the defective autophagic clearance observed in old Sh3px1 flies compared with controls, as assessed by accumulation of Ref(2)P (Figure 4C). We note here that Tak1 also displayed a marked increase in relative protein amount in these Sh3px1 flies compared with control (Figure 4C).

Having established that Sh3px1 strongly associates with Tab2, we next examined how loss of the sorting nexin affects the IMD response. Similar to the method already described for the $Tak1^{LIR1}$ flies, we used qPCR to assess the expression profiles of *AttA*, *DptB*, and *Dro* (Engström, 1999; Hanson et al., 2019; Lemaitre et al., 1997) in population samples from young (1-week-old adult) and old (2.5-week-old adult) $WT^{unc.}$ and Sh3px1 flies. Following analysis of our data, we observed that mRNA expression levels for all AMPs tested were elevated across all conditions relative to the 1-week-old $WT^{unc.}$ controls (Figure 4D). Moreover, although these fluctuated more in the older $WT^{unc.}$ flies compared with their young controls, they displayed a tendency for increase, in line with the gain-of-function phenotype of the innate immune system during aging (Franceschi et al., 2006; Salminen et al., 2008). We have previously reported persistently elevated levels of IMD-regulated AMP genes upon autophagy inhibition by loss of the core autophagy protein Atg8a in autophagy-deficient *Atg8a*-mutant flies (Tusco et al., 2017), which suggests an autophagy-dependent control of the

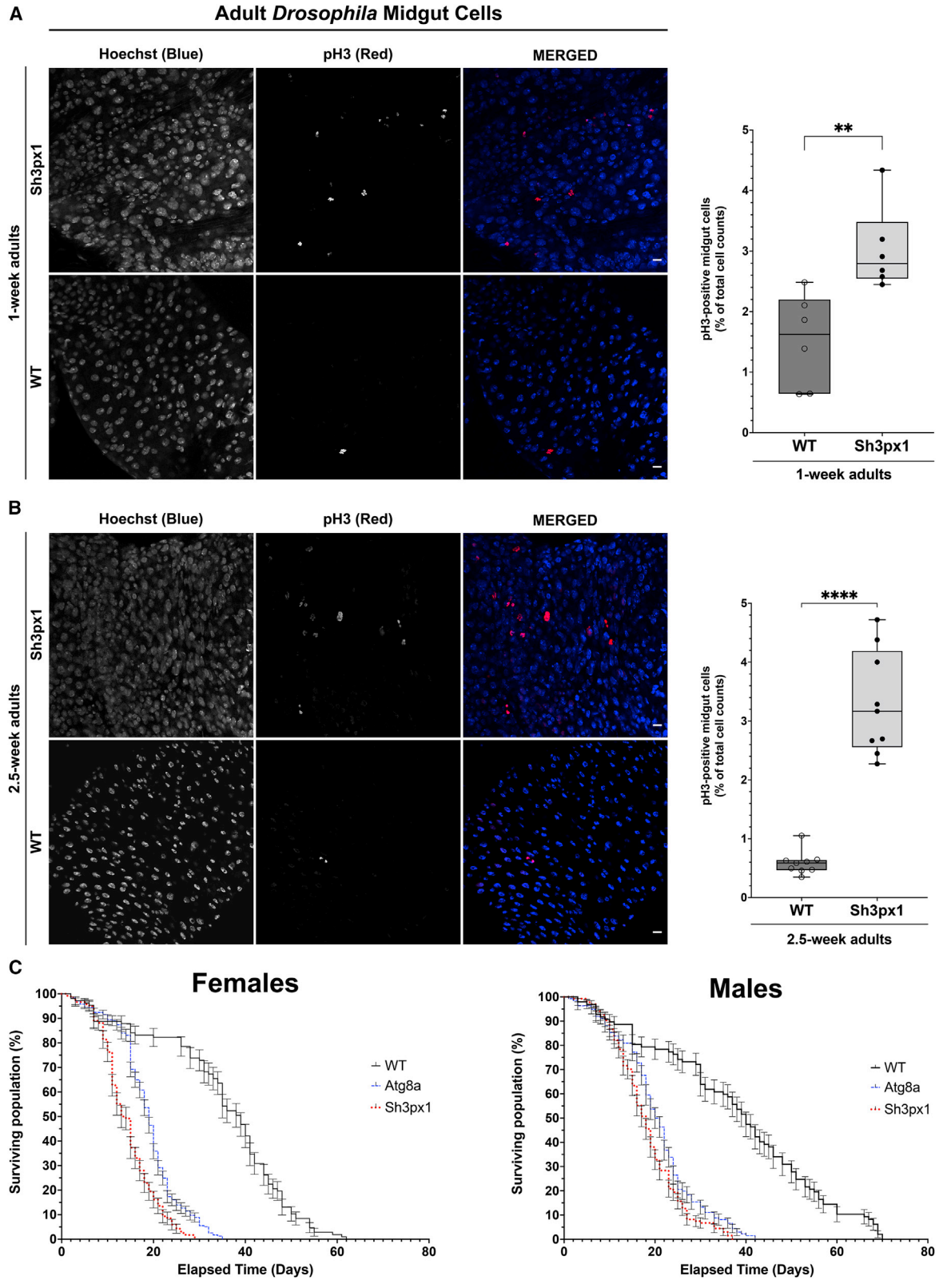

(legend on next page)

IMD pathway. Here, we observed that autophagy impairment by loss of the auxiliary component *Sh3px1* also promotes chronic IMD hyperactivation, as seen by the increased mRNA expression levels of *AttA*, *DptB*, and *Dro* (Figure 4D), corroborating the report of Zhang et al. (2019). It is interesting to note here that *Sh3px1*-deficient flies present with a phenotype regarding average lifespan and IMD pathway overactivation that is similar to *Atg8a* mutants (Tusco et al., 2017). This is in spite of *Sh3px1*-mutants exhibiting an arguably milder form of autophagy inhibition compared with Atg8a loss, as assessed by the lesser accumulation of the autophagy marker Ref(2)P observed in these flies (Figure 4C and as seen in Tusco et al., 2017, for *Atg8a*-mutants). The above showcases the close correlation between perturbations in autophagy and altered innate immune signaling.

In order to examine the physiological effect of systemic IMD upregulation in conventionally reared Sh3px1 flies, we assessed ISC hyperproliferation by immunostaining posterior midgut sections for phospho-Histone H3 (pH3), a specific marker for mitotic cells (Figures 5A and 5B). We also examined the longevity of Sh3px1 flies in survival assays along WT and Atg8a populations (Figure 5C). Despite using different *Sh3px1*-deficient flies in our experiments than Zhang et al. (2019) used in their work, our findings were still in line with the authors' observations, as both young and old Sh3px1 flies exhibited higher percentage ratios of pH3-positive cells compared with their respective age-matched controls (Figures 5A and 5B). In a similar fashion, both male and female Sh3px1 fly populations also displayed markedly shorter lifespans compared with WT controls, which were almost indistinguishable from the *Atg8a*-mutant flies used as a positive control for major autophagy impairment (Figure 5C).

In summary, these collective data showcase a role for Sh3px1 in the regulation of the IMD pathway by its ability to associate with Tab2. Loss of *Sh3px1* contributes to chronic challenge of the IMD innate immune response, as shown by the elevated protein levels for Tak1; the systemic mRNA amount of the IMD-regulated genes *AttA*, *DptB*, and *Dro*; and ISC hyperproliferation in the midgut. The above also correlated with a significantly compromised lifespan of *Sh3px1*-null flies. Altogether, our results suggest that, under basal conditions, Sh3px1 provides regulatory input on the IMD immune signaling in *Drosophila* by interacting with Tab2 at the tier of the apical Tak1/Tab2 complex.

DISCUSSION

As a basis for this work, the current study used the combinatory information obtained from the Atg8a-interacting proteins identified by high-throughput Y2H screening, together with the LIR motifs predicted on those proteins by the iLIR software (Kalvari et al., 2014). A list of the identified Atg8a-interacting proteins and their predicted LIR motifs are given in Figure S1 and Table S1 respectively. Of note, the Y2H results contained undescribed Atg8a-interacting proteins, as well as proteins that have previously been shown to interact with either Atg8a in *Drosophila* or the LC3/GABARAP family in mammals (Figure S2).

Autophagy and the innate immune response are two of the processes whose efficiencies are known to wane with age (López-Otín et al., 2013). However, where autophagy function progressively declines, innate immune responses become increasingly persistent, even in the absence of external inflammatory challenges, and consequently harder to terminate (Salminen et al., 2008; Yamaguchi and Otsu, 2012; Zerofsky et al., 2005). With regard to the latter, this is characteristic of the low-grade chronic inflammation phenotype that is tied to aging (Franceschi et al., 2017). Autophagy has been known to be an important facet of the modulatory mechanisms controlling innate immune responses (Nakahira et al., 2011; Prabakaran et al., 2018; Tusco et al., 2017), and perturbations in its function account for many pathologies associated with deregulated inflammatory signaling, such as neurodegeneration, auto-immune diseases, and cancer (Fésüs et al., 2011; Salminen et al., 2012; Shukla et al., 2019). In fact, our own previous work had identified the effector IKK complex of the *Drosophila* IMD pathway to be selectively removed by autophagy via the LIR motif-dependent interaction of its regulatory subunit Kenny, with Atg8a (Tusco et al., 2017). This is seen as part of the negative feedback mechanism, which dampens activation of the IMD cascade by targeting the IKK complex for degradation (Tusco et al., 2017).

Keeping in line with our goal of delineating the regulatory control of the innate immune system response by the housekeeping functions of selective autophagy, in this study we identified that the apical Ser/Thr kinase of the IMD pathway, Tak1, and its co-activating partner Tab2 (Kleino et al., 2005; Silverman et al., 2003; Vidai et al., 2001; Zhuang et al., 2006), interact with the autophagy protein Atg8a in *Drosophila*. In addition, we assign a role to the Atg8a-interacting sorting nexin Sh3px1, as a necessary mediator for the efficient targeting of the Tak1/Tab2 complex to autophagosomes. Sh3px1's requirement for the effective fine-tuning of ISC hyperproliferation has previously been reported (Zhang et al., 2019), but the mechanism and its potential interacting partners in the IMD pathway remain elusive. We characterize here that Sh3px1 strongly associates with the co-activator protein Tab2 of the Tak1/Tab2 signaling complex (Figures

Figure 5. Chronic inflammation and reduced lifespan of Sh3px1 flies

(A and B) Confocal imaging of posterior midgut sections from (A) 1-week adult and (B) 2.5-week adult female *Drosophila* WT and Sh3px1 flies. Staining performed for endogenous mitotic marker pH3 indicating hyper-proliferative ISCs. Scale bar: 10 μm. Corresponding quantification plot of pH3-positive ISCs percentage ratio to total cell counts shown on the right of each image panel. Data shown as median ± 95% CI in distribution boxplot with individual percentage ratios calculated per image (n = 6 [1 week], n = 9 [2.5 week]; n represents the number of individual midgut images analyzed per group; statistical analysis by equal variance unpaired t test [1 week] and unequal variance unpaired t test [2.5 week]; **p < 0.05; ****p < 0.0001).

(C) Survival assays for female (left) and male (right) Sh3px1 flies. WT and Atg8a flies used for controls. Data shown as percentage surviving population per time point ± SD (n = 6 independent biological repeats per genotype).

Genotypes for (A)–(C): w^{1118} (WT), $Sh3px^{10A/C1\ CRISPR\ E2}$ (Sh3px1).

Genotype for (C): $Atg8a^{KG07569}$ (Atg8a).

4A and 4B). Consistent with previous observations (Zhang et al., 2019), *Sh3px1*-deficient flies exhibit a chronic hyperproliferative phenotype in the midgut, as shown by the increased number of pH3-positive mitotic cells compared with controls, and have markedly reduced lifespans (Figure 5). Our own findings complement this picture by revealing that *Sh3px1*-deficient flies exhibit, in particular, chronically elevated levels of the IMD-regulated AMP genes *AttA*, *DptB*, and *Dro* (Figure 4D). Collectively, the above results underline that Sh3px1 is a necessary component of the modulatory network that prevents the IMD innate immune signaling from over-activating across the lifespan of flies.

We observed that both Tak1 and Tab2 interact directly with Atg8a. Our results show that the Tak1-Atg8a interaction is LIR/LDS dependent, and we proceeded to characterize the functional LIR motif of Tak1 to be the 667-EGWVVI-672 peptide (Figure 1). Tab2 binding of Atg8a appears by our findings to not be mediated, at least by a canonical LIR motif (Figures 3C and 3D). By using two recombinant Tab2 fragments, we can nevertheless report that the Atg8a-interaction domain of Tab2 is likely nested with amino acid region 1–336 of the full-length protein (Figure 3D). It is interesting to note that this region of Tab2 contains the CUE domain of the protein (Figure 3A), which facilitates Ub binding (Shih et al., 2003).

Sh3px1 and its mammalian homolog SNX18 are known for their involvement primarily in endocytosis; however, by virtue of their function in sensing and promoting membrane curvature, they operate in diverse membrane deformation events, such as endocytic trafficking, outgrowth formation, and autophagosome formation (Hicks et al., 2015; Knævelsrud et al., 2013; Park et al., 2010; Ukken et al., 2016). More specifically for autophagy, Sh3px1 promotes correct membrane bending during autophagosome formation (Knævelsrud et al., 2013), but it is not degraded itself by autophagy (Knævelsrud et al., 2013). It is therefore interesting to posit that, upon mounting of autophagy, Sh3px1 might sequester Tab2 in a multimer that dissociates the co-activator from Tak1 to attenuate the immune signaling of the Tak1/Tab2 complex. Of particular note here, among the markers of autophagy impairment and chronic inflammation of *Sh3px1* mutants (Figures 4 and 5), these flies also display evidence of elevated protein levels for Tak1 (Figure 4D). In this speculative mechanism, Tak1 binding of Atg8a might serve to retain the kinase on the autophagosome, while Tab2 and Sh3px1 binding with each other and with Atg8a could perhaps aid both in the tethering of Tak1 to the vesicle and its dissociation from an active signaling complex. Both the *Drosophila* and mammalian TAK1 are key nodal components that bifurcate into the JNK pathway, which controls cell proliferation, and they also induce necroptotic cell death upon overactivation (HuangFu et al., 2006; Lamothe et al., 2013; Mihaly et al., 2014; Silverman et al., 2003). It has also recently been shown that TAK1 in mammals can interact with SQTSM1/p62 and co-localize with the autophagy adaptor into distinct and degradation-resistant intracellular signaling complexes (Kehl et al., 2019). Based on the above examples that highlight Tak1/TAK1's multifaceted role in diverse signaling cascades, it may be reasonable to assume that an elaborate mechanism, with emphasis on disengaging the kinase from active signaling complexes, would benefit the maintenance of cellular homeostasis. It is also interesting to disclose here that the regulatory control innate immune signaling by selective autophagy seems, at least from our findings, to be specific to IMD, as the Toll pathway did not present evidence of overactivation during our work (Figure S6A).

We integrated our current interpretation of our findings into a working model regarding the control of the IMD pathway activation by selective autophagy, via the combinatory interactions of Tak1, Tab2, and Sh3px1 with Atg8a (Figure S6B). It is not yet clear whether Tak1 and Tab2 can interact with the same Atg8a molecule in a non-antagonistic manner, or bind proximal Atg8a moieties individually. The LIR1 motif of Tak1, as well as Sh3px1, seem to be required for the efficient downregulation of the multimer on the autophagosome, since loss of either results in chronic upregulation of the IMD pathway, as shown by qPCR (Figures 2E and 4D). Loss of Sh3px1 may in turn reduce efficient targeting of the Tak1/Tab2 complex to the autophagosome, thus leaving more Tak1/Tab2 active signaling complexes in the cytoplasm. The fact that all three proteins are capable, at least *in vitro*, of strongly and directly associating with Atg8a provides further evidence in support of a failsafe mechanism that dissociates active Tak1/Tab2 signaling complexes and targets at least Tak1 for autophagic degradation.

In summary, we have shown that autophagy plays an important role in the termination of the IMD innate immune signaling in *Drosophila*, by selectively degrading the Tak1/Tab2 complex. We show that this is achieved by the combined interactions of Tak1 and Tab2 with Atg8a, and further facilitated by the interactions of Sh3px1 with Tab2 and Atg8a. Our study highlights the physiological importance of selective autophagy in the innate immune response of metazoans and demonstrates the plasticity of its participating regulators.

Limitations of the study

TAK1 was identified as an Atg8a-interacting protein in Y2H screening. We also identified several other Atg8a-interacting proteins. However, the Y2H screening method cannot identify all interacting proteins for a given bait protein. We validated interactions of TAK1 with Atg8a and Trc with Atg8a. The current study does not characterize the interaction domain(s) of Trc with Atg8a and does not address the physiological role of Trc in autophagy.

STAR★METHODS

Detailed methods are provided in the online version of this paper and include the following:

- KEY RESOURCES TABLE
- RESOURCE AVAILABILITY
  - Lead contact
  - Materials availability
  - Data and code availability
- EXPERIMENTAL MODEL AND SUBJECT DETAILS
  - Fly husbandry and generation of transgenic flies
  - Creation of CRISPR Tak1^{LIR1} flies
- METHOD DETAILS
  - Yeast-2-hybrid screening
  - Plasmid constructs
  - Clonal mosaic analysis (FLPout/UAS-GAL4 system)

- Immunohistochemistry
- Mass spectrometry
- GST pulldown assays
- Protein extraction from tissue and western blot
- Primary antibodies and dilutions used
- Lifespan assays
- mRNA purification and qPCR sample preparation

- QUANTIFICATION AND STATISTICAL ANALYSIS
  - Confocal data
  - Immunoblots
  - Real-time qPCR and the ΔΔCt/Log2 method
  - Statistical analysis and figure creation software

SUPPLEMENTAL INFORMATION

Supplemental information can be found online at https://doi.org/10.1016/j.celrep.2021.110286.

ACKNOWLEDGMENTS

We thank Dr. G.B. Gonsalvez and Prof. G. Juhasz for gifting the Sh3px1 mutant and Atg8a mutant flies, respectively, and A. Torok for the fly food preparation. We thank Dr. Manolis Fanto for helpful discussions. The Bloomington *Drosophila* Stock Center contributed to this work by providing mutant and transgenic fly strains. We acknowledge Hybrigenics Services, Bestgene Inc., and Wellgenetics Inc. We also thank Abcam and Eurogentec for their aid in generating the Tak1 and Tab2 antibodies respectively. This work was supported by BBSRC grants BB/L006324/1 and BB/P007856/1 and Leverhulme Trust project grant RPG-2017-023 awarded to I.P.N. P.T. holds a PhD studentship funded by the Midlands Integrative Biosciences Training Partnership. A.S. acknowledges support by an Institutional Links grant (623760210), under the UK-Thailand Research and Innovation Partnership Fund. The grant is funded by the UK Department for Business, Energy and Industrial Strategy and delivered by the British Council. Work in the Meier laboratory is funded by Breast Cancer Now as part of Programme Funding to the Breast Cancer Now Toby Robins Research Center (CTR-QR14-007). P.M. acknowledges NHS funding to the NIHR Biomedical Research Center.

AUTHOR CONTRIBUTIONS

I.P.N. conceived the project. P.T. performed all the experiments. A.-C.J. prepared the plasmids for Y2H. S.P. did experiments related to Trc and TAB2 cloning. S.C. and M.G. did supplementary western blotting. A.S. provided resources and funding. P.M. did the mass spectrometry analysis. I.P.N. and P.T. composed the manuscript. All authors reviewed the manuscript and discussed the work.

DECLARATION OF INTERESTS

The authors declare no competing interests.

Received: April 30, 2021
Revised: December 7, 2021
Accepted: December 29, 2021
Published: January 25, 2022

REFERENCES

Alemu, E.A., Lamark, T., Torgersen, K.M., Birgisdottir, A.B., Larsen, K.B., Jain, A., Olsvik, H., Øvervatn, A., Kirkin, V., and Johansen, T. (2012). ATG8 family proteins act as scaffolds for assembly of the ULK complex: sequence requirements for LC3-interacting region (LIR) motifs. J. Biol. Chem. *287*, 39275–39290.

Basset, A., Khush, R.S., Braun, A., Gardan, L., Boccard, F., Hoffmann, J.A., and Lemaitre, B. (2000). The phytopathogenic bacteria *Erwinia carotovora* infects *Drosophila* and activates an immune response. Proc. Natl. Acad. Sci. U S A *97*, 3376–3381.

Besse, A., Lamothe, B., Campos, A.D., Webster, W.K., Maddineni, U., Lin, S.-C., Wu, H., and Darnay, B.G. (2007). TAK1-dependent signaling requires functional interaction with TAB2/TAB3. J. Biol. Chem. *282*, 3918–3928.

Birgisdottir, Å., Lamark, T., and Johansen, T. (2013). The LIR motif - crucial for selective autophagy. J. Cell Sci. *126*, 3237–3247.

Biteau, B., Karpac, J., Supoyo, S., DeGennaro, M., Lehmann, R., and Jasper, H. (2010). Lifespan extension by preserving proliferative homeostasis in *Drosophila*. PLoS Genet. *6*, 1–15.

Bjørkøy, G., Lamark, T., Brech, A., Outzen, H., Perander, M., Øvervatn, A., Stenmark, H., and Johansen, T. (2005). p62/SQSTM1 forms protein aggregates degraded by autophagy and has a protective effect on huntingtin-induced cell death. J. Cell Biol. *171*, 603–614.

Buchon, N., Broderick, N.A., Chakrabarti, S., and Lemaitre, B. (2009). Invasive and indigenous microbiota impact intestinal stem cell activity through multiple pathways in *Drosophila*. Genes Dev. *23*, 2333–2344.

Buchon, N., Silverman, N., and Cherry, S. (2014). Immunity in *Drosophila melanogaster*-from microbial recognition to whole-organism physiology. Nat. Rev. Immunol. *14*, 796–810.

Choi, H., Larsen, B., Lin, Z.Y., Breitkreutz, A., Mellacheruvu, D., Fermin, D., Qin, Z.S., Tyers, M., Gingras, A.C., and Nesvizhskii, A.I. (2011). SAINT: probabilistic scoring of affinity purification-mass spectrometry data. Nat. Methods *8*, 70–73.

Deretic, V. (2021). Autophagy in inflammation, infection, and immunometabolism. Immunity *54*, 437–453.

Engström, Y. (1999). Induction and regulation of antimicrobial peptides in *Drosophila*. Dev. Comp. Immunol. *23*, 345–358.

Fésüs, L., Demény, M.Á., and Petrovski, G. (2011). Autophagy shapes inflammation. Antioxid. Redox Signal. *14*, 2233–2243.

Franceschi, C., Bonafè, M., Valensin, S., Olivieri, F., De Luca, M., Ottaviani, E., and De Benedictis, G. (2006). Inflamm-aging: an evolutionary perspective on immunosenescence. Ann. N. Y. Acad. Sci. *908*, 244–254.

Franceschi, C., Garagnani, P., Vitale, G., Capri, M., and Salvioli, S. (2017). Inflammaging and 'Garb-aging'. Trends Endocrinol. Metab. *28*, 199–212.

Francis, V.A., Zorzano, A., and Teleman, A.A. (2010). DDOR is an EcR coactivator that forms a feed-forward loop connecting insulin and ecdysone signaling. Curr. Biol. *20*, 1799–1808.

Guo, L., Karpac, J., Tran, S.L., and Jasper, H. (2014). PGRP-SC2 promotes gut immune homeostasis to limit commensal dysbiosis and extend lifespan. Cell *156*, 109–122.

Hanson, M.A., Dostálová, A., Ceroni, C., Poidevin, M., Kondo, S., and Lemaitre, B. (2019). Synergy and remarkable specificity of antimicrobial peptides in vivo using a systematic knockout approach. eLife *8*, e44341.

Hicks, L., Liu, G., Ukken, F.P., Lu, S., Bollinger, K.E., O'Connor-Giles, K., and Gonsalvez, G.B. (2015). Depletion or over-expression of Sh3px1 results in dramatic changes in cell morphology. Biol. Open *4*, 1448–1461.

HuangFu, W.C., Omori, E., Akira, S., Matsumoto, K., and Ninomiya-Tsuji, J. (2006). Osmotic stress activates the TAK1-JNK pathway while blocking TAK1-mediated NF-κB activation: TAO2 regulates TAK1 pathways. J. Biol. Chem. *281*, 28802–28810.

Imler, J.-L., and Bulet, P. (2005). Antimicrobial peptides in *Drosophila*: structures, activities and gene regulation. In Mechanisms of Epithelial Defense (Karger), pp. 1–21.

Jacomin, A.C., and Nezis, I.P. (2016). Using fluorescent reporters to monitor autophagy in the female germline cells in *Drosophila melanogaster*. In Methods in Molecular Biology, I. Nezis, ed. (Humana Press Inc.), pp. 69–78.

Jain, A., Rusten, T.E., Katheder, N., Elvenes, J., Bruun, J.-A.A., Sjøttem, E., Lamark, T., and Johansen, T. (2015). P62/sequestosome-1, autophagy-related gene 8, and autophagy in *Drosophila* are regulated by nuclear factor erythroid 2-related factor 2(NRF2), independent of transcription factor TFEB. J. Biol. Chem. *290*, 14945–14962.

Jinek, M., Chylinski, K., Fonfara, I., Hauer, M., Doudna, J.A., and Charpentier, E. (2012). A programmable dual-RNA-guided DNA endonuclease in adaptive bacterial immunity. Science *337*, 816–821.

Johansen, T., and Lamark, T. (2011). Selective autophagy mediated by autophagic adapter proteins. Autophagy *7*, 279–296.

Johansen, T., and Lamark, T. (2020). Selective autophagy: ATG8 family proteins, LIR motifs and cargo receptors. J. Mol. Biol. *432*, 80–103.

Kalvari, I., Tsompanis, S., Mulakkal, N.C., Osgood, R., Johansen, T., Nezis, I.P., and Promponas, V.J. (2014). iLIR: a web resource for prediction of Atg8-family interacting proteins. Autophagy *10*, 913–925.

Kehl, S.R., Soos, B.A., Saha, B., Choi, S.W., Herren, A.W., Johansen, T., and Mandell, M.A. (2019). TAK 1 converts Sequestosome 1/p62 from an autophagy receptor to a signaling platform. EMBO Rep. *20*, e46238.

Kirisako, T., Ichimura, Y., Okada, H., Kabeya, Y., Mizushima, N., Yoshimori, T., Ohsumi, M., Takao, T., Noda, T., and Ohsumi, Y. (2000). The reversible modification regulates the membrane-binding state of Apg8/Aut7 essential for autophagy and the cytoplasm to vacuole targeting pathway. J. Cell Biol. *151*, 263–275.

Kirkin, V., Lamark, T., Sou, Y.S., Bjørkøy, G., Nunn, J.L., Bruun, J.A., Shvets, E., McEwan, D.G., Clausen, T.H., Wild, P., et al. (2009). A role for NBR1 in autophagosomal degradation of ubiquitinated substrates. Mol. Cell *33*, 505–516.

Kleino, A., Valanne, S., Ulvila, J., Kallio, J., Myllymäki, H., Enwald, H., Stöven, S., Poidevin, M., Ueda, R., Hultmark, D., et al. (2005). Inhibitor of apoptosis 2 and TAK1-binding protein are components of the *Drosophila* Imd pathway. EMBO J. *24*, 3423–3434.

Knævelsrud, H., Søreng, K., Raiborg, C., Håberg, K., Rasmuson, F., Brech, A., Liestøl, K., Rusten, T.E., Stenmark, H., Neufeld, T.P., et al. (2013). Membrane remodeling by the PX-BAR protein SNX18 promotes autophagosome formation. J. Cell Biol. *202*, 331–349.

Komatsu, M., Waguri, S., Chiba, T., Murata, S., Iwata, J.I., Tanida, I., Ueno, T., Koike, M., Uchiyama, Y., Kominami, E., et al. (2006). Loss of autophagy in the central nervous system causes neurodegeneration in mice. Nature *441*, 880–884.

Lamothe, B., Lai, Y., Xie, M., Schneider, M.D., and Darnay, B.G. (2013). TAK1 is essential for osteoclast differentiation and is an important modulator of cell death by apoptosis and necroptosis. Mol. Cell. Biol. *33*, 582–595.

Lemaitre, B., Reichhart, J.M., and Hoffmann, J.A. (1997). *Drosophila* host defense: differential induction of antimicrobial peptide genes after infection by various classes of microorganisms. Proc. Natl. Acad. Sci. U S A *94*, 14614–14619.

Li, J., Zhu, R., Chen, K., Zheng, H., Zhao, H., Yuan, C., Zhang, H., Wang, C., and Zhang, M. (2018). Potent and specific Atg8-targeting autophagy inhibitory peptides from giant ankyrins. Nat. Chem. Biol. *14*, 778–787.

López-Otín, C., Blasco, M.A., Partridge, L., Serrano, M., and Kroemer, G. (2013). The Hallmarks of aging. Cell *153*, 1194.

Mauvezin, C., Ayala, C., Braden, C.R., Kim, J., and Neufeld, T.P. (2014). Assays to monitor autophagy in *Drosophila*. Methods *68*, 134–139.

Mihaly, S.R., Ninomiya-Tsuji, J., and Morioka, S. (2014). TAK1 control of cell death. Cell Death Differ. *21*, 1667–1676.

Mizushima, N. (2007). Autophagy: process and function. Genes Dev. *21*, 2861–2873.

Myllymaki, H., Valanne, S., and Ramet, M. (2014). The *Drosophila* Imd signaling pathway. J. Immunol. *192*, 3455–3462.

Nakahira, K., Haspel, J.A., Rathinam, V.A.K.K., Lee, S.-J.J., Dolinay, T., Lam, H.C., Englert, J.A., Rabinovitch, M., Cernadas, M., Kim, H.P., et al. (2011). Autophagy proteins regulate innate immune responses by inhibiting the release of mitochondrial DNA mediated by the NALP3 inflammasome. Nat. Immunol. *12*, 222–230.

Nezis, I.P., Simonsen, A., Sagona, A.P., Finley, K., Gaumer, S., Contamine, D., Rusten, T.E., Stenmark, H., and Brech, A. (2008). Ref(2)P, the *Drosophila melanogaster* homologue of mammalian p62, is required for the formation of protein aggregates in adult brain. J. Cell Biol. *180*, 1065–1071.

Nowak, J., Archange, C., Tardivel-Lacombe, J., Pontarotti, P., Pébusque, M.J., Vaccaro, M.I., Velasco, G., Dagorn, J.C., and Iovanna, J.L. (2009). The TP53INP2 protein is required for autophagy in mammalian cells. Mol. Biol. Cell *20*, 870–881.

Pankiv, S., Clausen, T.H., Lamark, T., Brech, A., Bruun, J.-A.A., Outzen, H., Øvervatn, A., Bjørkøy, G., Johansen, T., Øvervatn, A., et al. (2007). p62/SQSTM1 binds directly to Atg8/LC3 to facilitate degradation of ubiquitinated protein aggregates by autophagy. J. Biol. Chem. *282*, 24131–24145.

Park, J., Kim, Y., Lee, S., Park, J.J., Park, Z.Y., Sun, W., Kim, H., and Chang, S. (2010). SNX18 shares a redundant role with SNX9 and modulates endocytic trafficking at the plasma membrane. J. Cell Sci. *123*, 1742–1750.

Parzych, K.R., and Klionsky, D.J. (2014). An overview of autophagy: morphology, mechanism, and regulation. Antioxid. Redox Signal. *20*, 460–473.

Prabakaran, T., Bodda, C., Krapp, C., Zhang, B., Christensen, M.H., Sun, C., Reinert, L., Cai, Y., Jensen, S.B., Skouboe, M.K., et al. (2018). Attenuation of c GAS - STING signaling is mediated by a p62/SQSTM 1-dependent autophagy pathway activated by TBK1. EMBO J. *37*, e97858.

Rutschmann, S., Jung, A.C., Zhou, R., Silverman, N., Hoffmann, J.A., and Ferrandon, D. (2000). Role of *Drosophila* IKKγ in a Toll-independent antibacterial immune response. Nat. Immunol. *1*, 342–347.

Ryu, J.H., Kim, S.H., Lee, H.Y., Jin, Y.B., Nam, Y. Do, Bae, J.W., Dong, G.L., Seung, C.S., Ha, E.M., and Lee, W.J. (2008). Innate immune homeostasis by the homeobox gene Caudal and commensal-gut mutualism in *Drosophila*. Science (80-) *319*, 777–782.

Salminen, A., Huuskonen, J., Ojala, J., Kauppinen, A., Kaarniranta, K., and Suuronen, T. (2008). Activation of innate immunity system during aging: NF-kB signaling is the molecular culprit of inflamm-aging. Ageing Res. Rev. *7*, 83–105.

Salminen, A., Kaarniranta, K., and Kauppinen, A. (2012). Inflammaging: disturbed interplay between autophagy and inflammasomes. Aging *4*, 166–175.

Scott, R.C., Juhász, G., and Neufeld, T.P. (2007). Direct induction of autophagy by Atg1 inhibits cell growth and induces apoptotic cell death. Curr. Biol. *17*, 1–11.

Shih, S.C., Prag, G., Francis, S.A., Sutanto, M.A., Hurley, J.H., and Hicke, L. (2003). A ubiquitin-binding motif required for intramolecular monoubiquitylation, the CUE domain. EMBO J. *22*, 1273–1281.

Shukla, A.K., Spurrier, J., Kuzina, I., and Giniger, E. (2019). Hyperactive innate immunity causes degeneration of dopamine neurons upon altering activity of Cdk5. Cell Rep. *26*, 131–144.e4.

Silverman, N., Zhou, R., Erlich, R.L., Hunter, M., Bernstein, E., Schneider, D., and Maniatis, T. (2003). Immune activation of NF-kappaB and JNK requires *Drosophila* TAK1. J. Biol. Chem. *278*, 48928–48934.

Stöven, S., Silverman, N., Junell, A., Hedengren-Olcott, M., Erturk, D., Engström, Y., Maniatis, T., and Hultmark, D. (2003). Caspase-mediated processing of the *Drosophila* NF-κB factor relish. Proc. Natl. Acad. Sci. U S A *100*, 5991–5996.

Sun, A., Wei, J., Childress, C., Shaw, J.H., Peng, K., Shao, G., Yang, W., and Lin, Q. (2017). The E3 ubiquitin ligase NEDD4 is an LC3-interactive protein and regulates autophagy. Autophagy *13*, 522–537.

Tanji, T., Hu, X., Weber, A.N.R., and Ip, Y.T. (2007). Toll and IMD pathways synergistically activate an innate immune response in *Drosophila melanogaster*. Mol. Cell. Biol. *27*, 4578–4588.

Tooze, S.A., Abada, A., and Elazar, Z. (2014). Endocytosis and autophagy: exploitation or cooperation? Cold Spring Harb. Perspect. Biol. *6*, a018358.

Tusco, R., Jacomin, A.C., Jain, A., Penman, B.S., Larsen, K.B., Johansen, T., and Nezis, I.P. (2017). Kenny mediates selective autophagic degradation of the IKK complex to control innate immune responses. Nat. Commun. *8*, 1264.

Ukken, F.P., Bruckner, J.J., Weir, K.L., Hope, S.J., Sison, S.L., Birschbach, R.M., Hicks, L., Taylor, K.L., Dent, E.W., Gonsalvez, G.B., et al. (2016). BAR-SH3 sorting nexins are conserved interacting proteins of Nervous wreck that organize synapses and promote neurotransmission. J. Cell Sci. *129*, 166.

Valanne, S., Wang, J.-H., and Rämet, M. (2011). The *Drosophila* toll signaling pathway. J. Immunol. *186*, 649–656.

Vidai, S., Khush, R.S., Leulier, F., Tzou, P., Nakamura, M., and Lemaitre, B. (2001). Mutations in the *Drosophila* dTAK1 gene reveal a conserved function for MAPKKKs in the control of rel/NF-κB-dependent innate immune responses. Genes Dev. *15*, 1900–1912.

Yamaguchi, O., and Otsu, K. (2012). Role of autophagy in aging. J. Cardiovasc. Pharmacol. *60*, 242–247.

Zerofsky, M., Harel, E., Silverman, N., and Tatar, M. (2005). Aging of the innate immune response in *Drosophila melanogaster*. Aging Cell *4*, 103–108.

Zhang, P., Holowatyj, A.N., Roy, T., Pronovost, S.M., Marchetti, M., Liu, H., Ulrich, C.M., and Edgar, B.A. (2019). An SH3PX1-dependent endocytosis-autophagy network restrains intestinal stem cell proliferation by counteracting EGFR-ERK signaling. Dev. Cell *49*, 574–589.e5.

Zhuang, Z.H., Sun, L., Kong, L., Hu, J.H., Yu, M.C., Reinach, P., Zang, J.W., and Ge, B.X. (2006). *Drosophila* TAB2 is required for the immune activation of JNK and NF-kappaB. Cell. Signal. *18*, 964–970.

STAR★METHODS

KEY RESOURCES TABLE

REAGENT or RESOURCE	SOURCE	IDENTIFIER
Antibodies		
Mouse anti-6xHis tag®	Abcam	Cat#ab18184; N/A
Rabbit anti-beta actin	Abcam	Cat#ab8227; RRID:AB_2305186
Rabbit anti-Cathepsin-L	Abcam	Cat#ab58991; RRID:AB_940826
Rabbit anti-Ref(2)P	Abcam	Cat#ab178440; N/A
Rabbit anti-Tak1 (*Drosophila*)	Abcam	Cat#ab2393353; N/A
Mouse anti-alpha tubulin	Sigma-Aldrich	Cat#T5168; RRID:AB_477579
Mouse anti-FLAG®(Clone M2)	Sigma-Aldrich	Cat#F1804; RRID:AB_262044
Goat anti-mouse IgG, CF 488A	Sigma-Aldrich	Cat#SAB4600042; RRID:AB_2532075
Goat anti-rabbit IgG, CF 568A	Sigma-Aldrich	Cat#SAB4600085; N/A
Goat anti-mouse HRP	Thermo Scientific	Cat#31450; RRID:AB_228307
Goat anti-rabbit HRP	Thermo Scientific	Cat#31460; RRID:AB_228341
Bacterial strains		
BL21(DE3) Competent *E. coli*	New England Biolabs	Cat#C2527I
Rosetta™ 2(DE3) Singles™ Competent Cells	Novagen	Cat#71400
Chemicals, peptides, and recombinant proteins		
GoTaq qPCR Master Mix	Promega	Cat#A6002
cOmplete™ EDTA-free protease inhibitor cocktails	Roche	Cat#04693132001
Glutathione Sepharose® 4B	Sigma-Aldrich	Cat#17-0756-01
Formaldehyde	Sigma-Aldrich	Cat#F8775
Phosphatase Inhibitor Cocktail	Sigma-Aldrich	Cat#P5726
Critical commercial assays		
QuickChange II Site-Directed Mutagenesis Kit	Agilent	Cat#200523
DreamTaq DNA Polymerase	Thermo Scientific	Cat#K1081
PureLink™ RNA mini kit	Thermo Scientific	Cat#12183025
RevertAid cDNA Synthesis Kit	Thermo Scientific	Cat#K1622
Deposited data		
Drosophila Atg8a-interacting and LIR-containing proteome list	This paper	Table S1
Experimental models: cell lines		
Drosophila S2 Cells	Thermo Fisher	Cat#R69007
Experimental models: organisms/strains (*Drosophila melanogaster*)		
w^{1118}	Bloomington *Drosophila* Stock Center	Cat#3605
yw hs-FLP Atg8a^{KG07569}	Gift from G. Juhasz (Scott et al., 2007)	Atg8a[KG07569]
yw hs-flp;UAS-mCherry-Atg8a;Ac> CD2> GAL4	Laboratory of I.Nezis (Tusco et al., 2017)	N/A
Sh3px1^{10A}	Gift from G.B. Gonsalvez (Ukken et al., 2016)	N/A
Sh3px1 ^{C1}	Gift from G.B. Gonsalvez (Ukken et al., 2016)	N/A
UAS-3xFLAG:Tak1^{WT}	This paper, created by P-element-mediated recombination (BestGene Inc.)	N/A

(*Continued on next page*)

Continued		
REAGENT or RESOURCE	SOURCE	IDENTIFIER
UAS-3xFLAG:Tak1^{LIR1}	This paper, created by P-element-mediated recombination (BestGene Inc.)	N/A
w^{1118}; Tak1$^{W669A/I672A}$/FM7A (Tak1 ^{LIR1})	This paper, created by CRISPR-mediated recombination (WellGenetics Inc)	N/A
Oligonucleotides		
Primers for AMP mRNA expression (see STAR Methods: "mRNA Purification and qPCR sample preparation")	This paper	N/A
Primers for creating recombinant Tak1, Tab2 and mutant isoforms	This paper	Table S1
Recombinant DNA		
Plasmid: pET28a(+)	Novagen	Cat#69864
Plasmid: Gateway^{TM} pDEST^{TM}15	Thermo Fisher	Cat#11802014
Software and algorithms		
iLIR database	Kalvari et al. (2014)	http://repeat.biol.ucy.ac.cy/iLIR
AtgCOUNTER (ImageJ/Fiji macro)	Jacomin and Nezis (2016)	https://imagej.nih.gov/ij/
SAINT	Choi et al. (2011)	http://saint-apms.sourceforge.net/Main.html

RESOURCE AVAILABILITY

Lead contact

Additional information and requests for reagents and protocols should be directed to and will be fulfilled by the lead contact, Prof. Ioannis Nezis (I.Nezis@warwick.ac.uk).

Materials availability

All the materials used in this study are publicly available. Please contact Prof. Ioannis Nezis for requests.

Data and code availability

- All data generated and reported in this paper is available from the lead contact upon request.
- This paper does not report original code. The code for "AtgCOUNTER" is available in Jacomin and Nezis (2016).
- Any additional information required to reanalyse the data reported in this paper is available from the lead contact upon request.

EXPERIMENTAL MODEL AND SUBJECT DETAILS

Fly husbandry and generation of transgenic flies

Flies used in experiments were kept at 25°C, 70% humidity and raised on a cornmeal based-diet. The *w^{1118}* (#3605) flies were used as the wild type control group for most experiments and were obtained from the Bloomington *Drosophila* stock center. The *yw hs-FLP Atg8a^{KG07569}* (Atg8a) flies were a kind gift from G. Juhasz (Scott et al., 2007). G.B.Gonsalvez kindly donated the *Sh3px1^{10A}* and *Sh3px1^{C1}* null-alleles. The two strains were crossed to each other in order to manifest the full *Sh3px1*-mutant phenotype (Sh3px1 in text) in the F1 progeny, which we subsequently used for our experiments. For the mutant mosaic analysis (FLPout/UAS-GAL4 mitotic recombination), the *yw hs-flp;UAS-mCherry-Atg8a;Ac>CD2>*GAL4 line was used (gift form G. Juhasz). The transgenic *UAS-FLAG:Tak1^{WT}* and *UAS-FLAG:Tak1^{LIR1}* lines (full construct name: *pUASattB/UAS-3xFLAG:Tak1^{WT}* and *pUASattB/UAS-3xFLAG:Tak1^{LIR1}* respectively) were created using the *attB/attP* site-specific recombination. The selected *attP*-landing site (*attP40*) for the attB-vector was the same for both fly lines created in this manner, ensuring that transgenic constructs would in turn be expressed in similar levels to allow for normalized comparisons to be made between the two groups. The recombinant vectors were shipped to Best Gene Inc. (USA), who performed the embryo microinjections and generated the final transgenic flies according to standard practices.

Creation of CRISPR Tak1^{LIR1} flies

Tak1 LIR$^{W669A/I672A}$ CRISPR flies were created using site-directed mutagenesis and genome editing via CRISPR/Cas9 homology-dependent repair, done by Wellgenetics Inc. (Taiwan) (Jinek et al., 2012). The creation of the CRISPR *Tak1^{LIR1}* flies was performed

in 4 steps. First, the target gene was mutated at the desired precise locations by site-directed mutagenesis. Then an excisable fluorescent reporter was introduced within the target gene by P element transposition (PBac-DsRed). This disrupts the gene initially but serves as a screening tool to validate those fly strains, where the construct has successfully integrated within the genome at the desired site, following injections of embryos. Then micro-injections were performed on *Drosophila* embryos, and replacement of endogenous dTAK1 with the transgenic construct was directed by CRISPR/Cas9-mediated homology-dependent repair. Finally, the entire PBacDsRed element is excised, effectively reconstituting the functional gene, which is now the dTAK1 LIR1 mutant form, expressed across the entire genome of the selected fly strains.

METHOD DETAILS

Yeast-2-hybrid screening

Full-length Atg8a coding sequence was amplified by PCR from pPW-mCherry-ATG8a plasmid (fwd: 5′-CCGGAATTCATGAAGTTC CAATACAAGGAGGAGC-3′; rev: 5′-TTACGGCATGGCCAAAATTAACTAATAATAAGAGCTCCGG-3′) and ligated into pGEX-4T-1 plasmid following EcoRI/XhoI restriction enzymes digestion. Individual clones were checked by restriction enzyme digestion and constructs that have successfully inserted Atg8a were sent for sequencing.

For the yeast two-hybrid screen we used *Drosophila* Atg8a (1-121), as a LexA-bait (pB27) and an inducible LexA-bait fusion (pB31), performed on *Drosophila* instar larvae library by Hybrigenics Servises (Evry, France).

Plasmid constructs

The plasmid vectors, along with the relevant primers used in this study to make the recombinant constructs and the inactive LIR motif isoforms, are listed in Table S1, with the exception of GST:Atg8a^{WT} and GST:Atg8a$^{LDS\ (K48A/Y49A)}$ constructs (Tusco et al., 2017). PCR products were amplified from cDNA using Dream-Taq DNA polymerase (Thermo Fisher, K1081). Recombinant plasmids were made by conventional restriction enzyme-based cloning. Point-mutants were generated using the QuickChange II site-directed mutagenesis (Agilent, 200523) according to manufacturer's protocol. Oligonucleotides for mutagenesis, RT-PCR, qPCR and DNA sequencing were from IDT. Plasmid constructs were verified by conventional restriction enzyme digestion and/or by DNA-sequencing with Eurofins Genomics.

Clonal mosaic analysis (FLPout/UAS-GAL4 system)

We employed the FLPout/UAS-GAL4 system of *cis*-chromosomal recombination to generate a mosaic of mutant clones in the larval fat body, against a background of original genotype cells. Following this technique, the GAL4 expressing cells were generated spontaneously under normal incubation conditions of the flies. Fat bodies were subsequently dissected from L3 larvae 4 days after egg laying.

Immunohistochemistry

Fly tissues were dissected in PBS and fixed for 30 min in 4% formaldehyde at room temperature. Blocking, as well as primary/secondary antibody incubations were performed in PBT (0.3% BSA • 0.3% Triton-X100 in PBS). Primary and secondary antibodies were incubated overnight at 4°C, or for 2 h at room temperature, in PBT.

The following primary antibodies were used: mouse anti-FLAG® M2 (Sigma F1804, 1:1000), mouse anti-mono/polyubiquitinylated conjugates (Enzo® BML-PW8810, 1:1000), rabbit anti-pH3 (Millipore #06-570, 1:1000), rabbit anti-cathepsin L (Abcam ab58991, 1:1000) and rabbit anti-Tak1 (Abcam ab23953, 1:100).

Secondary fluorophore-conjugated antibodies were from Sigma: goat anti-mouse IgG, CF^{TM}488A (SAB4600042, 1:1000), and goat anti-rabbit IgG, CF^{TM}568A (SAB4600085, 1:1000). The Hoechst 33342 DNA staining dye (New England Biolabs #4082, 1:1000 in PBS) was used to visualize nuclei. Washes were performed in PBW (0.1% Tween-20 in PBS).

All images were acquired in Carl Zeiss LSM710 or LSM880 confocal microscopes, using a 63x Apochromat objective.

Mass spectrometry

To identify interactors of Tab2, we undertook a proteomic-based approach using Tab2 as affinity reagent in *Drosophila* S2 cells (Thermo Fisher, R69007). Tab2 was fused to 2x-HA tags and expressed in S2 cells. HA-tagged proteins were purified, and the presence of co-purified proteins was determined via mass spectrometry. Prior to mass spectrometry analysis eluted protein complexes were digested with Trypsin and peptides were purified using C18 Microspin columns (Harvard Apparatus) according to the manufacturer protocol. LC-MS/MS analysis was performed on a dual pressure LTQ-Orbitrap mass spectrometer (Thermo Scientific), which was connected to an electrospray ion source (Thermo Scientific).

Peptide separation was carried out using an easy nano-LC systems (Proxeon Biosystems) equipped with an RP-HPLC column packed with C18 resin (Magic C18 AQ 3 μm; Michrom BioResources). A 0.3 μL/min linear gradient from 96% solvent A (0.15% formic acid • 2% acetonitrile) and 4% solvent B (98% acetonitrile • 0.15% formic acid) to 40% solvent B over 40 min. The data acquisition mode was set to obtain one high-resolution MS scan in the FT part of the mass spectrometer at a resolution of 60,000 FWHM followed by MS/MS scans in the linear ion trap of the 20 most intense ions. Raw files were converted to the mzXML format, and searched against the human Swissprot protein database. Further data processing including SAINT was carried out as described previously (Choi et al., 2011).

GST pulldown assays

Both, the GST-fusion bait, and the His-labelled prey proteins were expressed in *Escherichia coli* BL21 Rosetta (DE3) (Novagen, 71400) and incubated in liquid cultures at 37°C, 150 rpm. Optical density (OD) at 600nm was used as a readout for culture density and measured at regular intervals. Optimal culture density for BL21(DE3) was reached at OD^{600} 0.5–0.6. At this point we induced protein expression by adding IPTG to the liquid culture, at a final concentration of 0.5 mM and incubating the cultures at 20°C, 150 rpm, for a further16 h. Bacteria were pelleted and re-suspended in lysis buffer (25 mM Tris pH 7.4 • 100 mM NaCl • 2 mM EDTA) additionally supplemented with 0.01% β-mercaptoethanol, and 1 μg/μL lysozyme (final concentrations). Cell integrity was disrupted by sonication using an EpiShear™ Probe Sonicator (in pulses 10sec ON, 5 sec OFF, 30% amplitude) for 2 min per sample. Protein content was collected as the supernatant of the following centrifugation at 20,000 rpm, 4°C for 20 min.

Both the GST-bait and His-prey lysates were incubated with Glutathione Sepharose® 4B (Sigma, 17-0756-01) for 30 min at 4°C. Subsequent washes were carried out in High Salt (25 mM Tris pH 7.4 • 500 mM NaCl • 2 mM EDTA) and Low Salt wash buffers (25 mM Tris pH 7.4 • 50 mM NaCl • 2 mM EDTA). After the washes each pre-cleared His-prey lysate was equally distributed to its respective GST bait-enriched beads and samples were co-incubated for 2 h at 4°C. They were subsequently washed with 0.01%-mercaptoethanol-supplemented lysis buffer, and Imidazole buffer (lysis buffer recipe + 10 mM imidazole). In preparation for gel loading, samples were finally re-suspended in equal volume of 2x Laemmli solution and denatured at 80°C for 10 min, prior to SDS-PAGE and subsequent Western Blot.

Oligonucleotides used to generate recombinant or point mutant constructs (shown in 5′→ 3′ direction).

DNA insert	Target vector	5′- forward primer	3′- reverse primer
3xFLAG	pUASattB	CCGGAATTCATGGACTACAAAGACC	CCGCTCGAGTCGGTACCGGAT
Tak1	pUASattB/*3xFLAG*	CCGCTCGAGATGGCCACAGCATC	GCTCTAGACTACGCATTGTGATGCGG
Sh3px1	pET28a	CCGGAATTCATGACCTCGTACGTG	CCCAAGCTTCTACTCAATCTGACGGC
Tab2	pGEX	TCCCCCCGGGTATGGCGGCTACAC	CCGCTCGAGTTAT GTATGCAGAGCGTACG
Tak1	pET28a	CCGGAATTCATGGCCACAGCATCG	CCCAAGCTTCTACGCATTGTGATGC
Tak1 LIR1	pET28a/*Tak1*	GAGTCCGTGGAAGAAGGCGCGGT GGTCGCCCCACCGCATCACAATG	CATTGTGATGCGGTGGGGCGACC ACCGCGCCTTCTTCCACGGACTC
Tak1 LIR2	pET28a/*Tak1*	CACCGACACATGGCCAAGGAGGCC CTGAGCGCCGACACGAACCTCTAC	GTAGAGGTTCGTGTCGGCGCTCAG GGCCTCCTTGGCCATGTGTCGGTG
Tab2	pET28a	CCCAAGCTTATATGGCGGCTACACCAC	CCGCTCGAGTTATGTATGCAGAGCGTAC
Tab2 LIR1	pET28a/*Tab2*	CTGGTGGACGCAAGAGC GCCACCTCGGCCAATCTCACCCTG	CAGGGTGAGATTGGCCG AGGTGGCGCTCTTGCGTCCACCAG
Tab2 LIR2	pET28a/*Tab2*	CGTACGCGCGACGCT CGCAGCGCTGACTTTCCGCCGAC	GTCGGCGGAAAGTCAG CGCTGCGAGCGTCGCGCGCGTACG

Protein extraction from tissue and western blot

Whole fly samples consisting of age-matched individuals at an even male: female ratio were used to extract total protein content using motorized mortar and pestle. Lysis buffer (120 mM NaCl • 50 mM Tris-HCl pH 6.8 • 50 mM NaF • 1 mM benzamidine • 1 mM EDTA • 1 mM EGTA • 1 mM Na_3VO_4 • 15 mM $Na_4P_2O_7$ • 1% Igepal/NP-40) was supplemented with additional inhibitors for various proteases (cOmplete™ Mini, EDTA-free Protease Inhibitor Cocktail, Roche 04693132001) and phosphatases (Phosphatase Inhibitor Cocktail 2, Sigma P5726). All protein samples (whole fly lysates and co-immunoprecipitation eluates) were denatured for 10 min at 80°C. Gel-loading samples for SDS-PAGE were made at 100 μg total protein concentration and we were loading 5–10 μg of protein each time per well. Western Blot transfer was onto either nitrocellulose or PVDF membranes (cold wet transfer in 10% ethanol for one hour at 100V). Membranes were blocked in 5% BSA in TBST (0.1% Tween-20 in TBS) for 1 h at room temperature (RT). Primary antibodies were diluted in TBST and incubated overnight at 4°C, or for 2 h at room temperature, with gentle agitation. All subsequent washes were performed in TBST for 10–15 min per wash. Secondary HRP-coupled antibodies were diluted in 1% BSA-TBST and incubated for 45 min at RT. ECL mix was applied for 2 min at RT in dark conditions.

Primary antibodies and dilutions used

Obtained from Abcam: anti-Tak1 (ab239353, 1:300; created in collaboration with the I.Nezis lab), anti-Ref(2)P (ab178440, 1:1000), anti-beta Actin (ab8227, 1:2000), anti-6xHis (ab18184, 1:2000). Antibodies obtained from Developmental Studies Hybridoma Bank Iowa City: anti-Cactus (3H12, 1:72) and anti-Dorsal (7A4, 1:10). Other suppliers: anti-GST (Santa Cruz B-14 SC-138, 1:2000), anti-Tab2 (Eurogentec ZGB19056, 1:500). The anti-Tab2 antibody, was created by purified His:Tab2 from bacterial cultures, and used for immunizing rabbit hosts (injections performed by Eurogentec).

Secondary HRP-coupled secondary antibodies were from Thermo Scientific: anti-mouse HRP (#31450, 1:5000), and anti-rabbit HRP (#31460, 1:5000).

Lifespan assays

We used the Kaplan-Meier method to measure lifespan of flies, which estimates survival probability of each risk group according to daily death events counted. Male and female flies were collected within 24 h from hatching and cohorts of 20–25 flies were maintained on standard or autoclaved/antibiotics supplemented *Drosophila* food at 25°C in a humidified incubator. Flies were transferred into new tubes every 2–3 days. Dead events were recorded daily. Survival curves were constructed in Prism (GraphPad, version 9.1.0) and we used the Mantel-Cox test for statistical comparisons.

mRNA purification and qPCR sample preparation

Flies were raised under normal conditions and unchallenged by additional microbial load, other than the microbial population normally present in conventional fly food and growth conditions. As a positive control for the transient upregulation of the IMD pathway in response to acute microbial infection, WT flies were subjected to 4hrs starvation, before transferring to food-containing tubes enriched with the mild pathogenic Gram^{-ve} bacteria *Ecc15* (Basset et al., 2000), for natural infection via oral intake. These flies were then microbially challenged, for 6hrs at 29°C to induce AMP gene expression.

Isolated mRNA from whole-fly samples consisting of 10 age-matched and evenly mixed male/female flies per condition, was used to reverse-transcribe cDNA for each gene of interest. All procedures were performed according to manufacturer's guidelines. RNA was extracted using an Invitrogen PureLink^{TM} RNA Mini Kit (Thermo Fisher, 12183025). Subsequent steps were performed using 1μg of total RNA. Genomic DNA was removed by DNAse I digestion (Thermo Fisher, EN0521). For cDNA synthesis we used the RevertAid RT Reverse Transcription Kit (Thermo Fisher, K1622). qPCR reaction sample were made with the Promega GoTaq® qPCR Master Mix (Promega, A6002). The sequences of the forward and reverse primers used in qPCR are given below (in 5' → 3' direction):

Rp49 F (*housekeeping gene*): GCTAAGCTGTCGCACAAATG
Rp49 R (*housekeeping gene*): CGATCTCGCCGCAGTAAA
AttA F: GATGGACGTGCTAATCTCTG
AttA R: GGCTTAGCCGAAATGATGAG
DptB F: AGTTCACCATTGCCGTCGCC
DptB R: GTAGGTGTAGGTGCTTCCCA
Dro F: TCCACCACTCCAAGCACAATG
Dro R: ACACATCTTTAGGCGGGCAG

Prior to use, we performed a 1:50 working dilution of the cDNA template. Final volume in each well on the qPCR plate per reaction was 25 μL (20 μL primer reaction mix +5 μL cDNA template). qPCR was performed on a Stratagene Mx3005P (Agilent Technologies) system. The thermal profile setup for the qPCR assay was as follows:

Initial Denaturing (1 cycle): 95°C for 5 min
Denature/Annealing (45 cycles): 95°C for 15 s, then 60°C for 40 s
Final Melt Curve (1 cycle): 95°C for 1 min, 60°C for 30 s, then 95°C for 30 s
Hold at 10°C

QUANTIFICATION AND STATISTICAL ANALYSIS

All information regarding data representation, statistical test used, *n* number, p value reporting and calculated significance, is found in the figure legends.

Confocal data

All confocal images were post-processed in Fiji/ImageJ (version 2.1.0/1.53c) for colocalization and quantification purposes. Signal co-localization in Figures 1C and S4 was assessed by Pearson's correlation co-efficient (R) within set regions of interest (ROIs) of the total image (autophagosomes for Figure 1C; lysosomes for Figure S4). To identify ROIs, we used a semi-automated method termed "AtgCOUNTER" (Jacomin and Nezis, 2016). We obtained a total R value for all regions of interest identified per studied image. To calculate the Tak1^{+ve} puncta (Figures 2C and S5), as well as measure the total and pH3^{+ve} cell numbers, used for estimating the pH3^{+ve}-cell percentages (Figures 5A and 5B), we utilized the Threshold, Analyze Particles, and Cell Counter plugins available with the Fiji/ImageJ software. The number of Tak1 puncta per fat body image was normalized to the image area (Figures 2C and S5). For Figures 5A and 5B, percentages were obtained by dividing the number of pH3^{+ve} cells per midgut section over the total cell number for the same section.

Immunoblots

Band thickness for all proteins of interest and loading controls was measured as area under pixel intensity curves, generated in Fiji/Image J. For the duplet bands seen for Tak1 (Figures 2A and 4C) and Cactus (Figure S6), the entire band area shown was used for quantification. For Dorsal (Figure S6) the lower molecular weight band was used to calculate pixel intensity. For a cross-sample comparisons, we normalized the data by dividing the intensity value of each protein of interest per sample with the intensity values of their

respective loading controls. For the GST Pulldown assays the loading controls were the GST-baits visualized by Ponceau S (Figures 1B, 3C, 3D, and S3A) or anti-GST antibody (Figure 4B) staining, while actin or tubulin were used as loading controls for all other immunoblot experiments shown in this work. The value of the selected control group for each assay was further used as the reference to calibrate all other normalized values by dividing each group of interest's value over the control group (Control group's subsequent calibrated value set to 1; for log2-fold transformation reference group's threshold value is set to 0). We used the Shapiro-Wilk test to examine if data met the normality criteria before selecting whether a parametric or non-parametric test should be used. For statistical comparisons of each group of interest with the reference condition, we used a one-sample t test, or equivalent non-parametric where appropriate. For comparisons of groups of interest with each other we used Student's t-test (2 groups), or one-way ANOVA if comparing $\geq$3 groups, or equivalent non-parametric tests.

Real-time qPCR and the ΔΔCt/Log2 method

For all qPCR experiments performed in this study, each experimental condition was loaded in triplicate wells (3 technical repeats) and the associated results were averaged. We utilized the MxPro software (Agilent Technologies) to extract the cycle-to-threshold (Ct) values measured by the qPCR assay for all studied genes. *Rp49* was used as the reference gene for the within-group normalization of data, subtracting the Ct^{Rp49} from each Ct of the AMPs tested (ΔCt). Similarly, the 1-week $WT^{unc.}$ flies were used as the overall control group, where all AMP ΔCts were calibrated to across conditions (ΔΔCt; Control group's subsequent ΔΔCt threshold value = 0; no change in expression) The ΔΔCt values represent the log2 fold-change in gene expression. These ΔΔCt/log2 fold-change values were used for all subsequent statistical comparisons and to depict AMP expression in the associated graphs shown herein.

Statistical analysis and figure creation software

The GraphPad Prism 9 software (version 9.1.0) was used to generate all graphical representations of data shown in this work, as well as to perform all the statistical test analyses. Compound figures were assembled in Adobe Photoshop 2020 (version 21.2.5).